JOURNAL OF MOLECULAR SPECTROSCOPY **158,** 208–236 (1993)

Laser and Fourier Transform Spectroscopy of PtH and PtD

MICHAEL C. MCCARTHY [1] AND ROBERT W. FIELD

Department of Chemistry, Massachusetts Institute of Technology, Cambridge, Massachusetts 02139

AND

ROLF ENGLEMAN, JR.,[2] AND PETER F. BERNATH[3]

Department of Chemistry, University of Arizona, Tucson, Arizona 85721

Three new bands of PtH and three new bands of PtD have been rotationally analyzed using laser excitation and Fourier transform spectroscopy. For both PtH and PtD, every band so far identified by laser spectroscopy originates from an $\Omega = 2.5$ lower state, which is assigned as the ground state. For the PtH band at 4367 Å, the upper state was found to be an $\Omega' = 1.5$ state which has been previously observed. From the dispersed fluorescence pattern from this $\Omega' = 1.5$ state and previous emission results we have been able to measure the spin–orbit interval between the $X\,\Omega = 1.5$ and $X\,\Omega = 2.5$ ground state components as 3224.9 (± 0.1) cm^{-1}. The corresponding $\Omega' = 1.5$–$X\,2.5$ (0, 0) band of PtD has also been identified at 4358 Å and has allowed us to measure a spin–orbit interval of 3228.5 (± 0.1) cm^{-1} between the $X\,\Omega = 1.5$ and $X\,\Omega = 2.5$ ground state components. Although these intervals are much larger than the previously estimated value of 1200 cm^{-1} by Kaving and Scullman, they are in better agreement with ab initio calculations and the large atomic Pt spin–orbit ζ_{5d} coupling constant. Hyperfine splittings due to the $I = \frac{1}{2}$ nuclear spin of ^{195}Pt have been observed in both the ground state and all of the upper states. In addition, isotope splittings have been resolved for several of the upper states. Using Fourier transform spectroscopy a new band system of PtH was found in emission in the near-infrared region around 8400 cm^{-1}. The lower state has been identified as the $X\,1.5$ ground state component and the upper state, located at 11 581.6 (± 0.2) cm^{-1}, is an $\Omega' = 1.5$ state of $^2\Pi_{3/2}$ parentage as predicted by theory. A small, low-J perturbation in the $\Omega' = 1.5$–$X\,\Omega'' = 1.5$ (0, 0) transition of PtD has allowed an independent estimate of 3227 (± 3) cm^{-1} for the $X\,\Omega = 1.5$–$X\,\Omega = 2.5$ ground state spin–orbit interval, which is in excellent agreement with laser excited dispersed fluorescence data. The results of both laser excitation and Fourier transform spectroscopy confirm the assignment of $X\,2.5$ as the ground state and have enabled all the known states of PtH to be linked in energy, including six of the ten lowest lying electronic states which are components of the Pt d^9 [^2D] H supermultiplet.

I. INTRODUCTION

The first spectra of gas-phase PtH were recorded in absorption by Scullman in 1964 (*1*). Seven red-degraded bands belonging to two $^2\Delta_{5/2}$–$^2\Delta_{5/2}$ transitions were rotationally analyzed. The ground state of PtH, like NiH, was found to be an inverted $^2\Delta_i$ state. In 1971, Kaving and Scullman succeeded in observing six additional PtH bands in emission; three belonging to a $^2\Delta_{3/2}$–$X\,^2\Delta_{3/2}$ subsystem and another three belonging to a $^2\Phi_{7/2}$–$X\,^2\Delta_{5/2}$ subsystem (*2, 3*). Although no intercombination bands linking the $\Omega'' = 2.5$ and $\Omega'' = 1.5$ $X\,^2\Delta$ components were identified, Kaving and Scullman estimated

[1] AT&T Bell Laboratories Ph.D. Scholar.

[2] Current address: Department of Chemistry, University of New Mexico, Albuquerque, NM 87131.

[3] Also Department of Chemistry, University of Waterloo, Waterloo, Ont., Canada N2L 3G1.

0022-2852/93 $5.00

the separation between the $X^2\Delta_{3/2}$ and the $X^2\Delta_{5/2}$ components to be about 1200 cm^{-1}. More recently, Scullman and co-workers have analyzed the corresponding band systems of PtD (*4–6*).

PtH has been the subject of several ab initio calculations (*7–11*). Third-row transition-metal species pose a computational challenge for theoreticians due to increased relativistic effects manifested as spin–orbit coupling and correlation effects. In the recent, most accurate calculation by Balasubramanian and Feng (*11*), potential energy curves and spectroscopic constants of 11 low-lying electronic states of PtH were computed. Their results indicate that spin-orbit effects are even more significant for PtH than for NiH. With the exception of the $X^2\Delta_{5/2}$ ground state, all of the electronic states are very strongly mixed. The ab initio calculation places the $X\Omega = 1.5$ ($X^2\Delta_{3/2}$) state 4200 cm^{-1} above the $X\Omega = 2.5$ ($X^2\Delta_{5/2}$) ground state.

In this paper, we report the analysis of three new red-degraded bands of PtH and three new red-degraded bands of PtD. One band of PtH and one band of PtD were recorded by laser excitation spectroscopy, and two bands of both PtH and PtD were observed in infrared emission by Fourier transform spectroscopy. The PtH band observed by laser excitation spectroscopy, which is assigned as a $\Omega' = 1.5$–$X\Omega'' = 2.5$ (0, 0) transition, has allowed us to measure directly the spin–orbit interval between the $X\Omega = 1.5$ and $X\Omega = 2.5$ ground state components using the technique of dispersed fluorescence. This intercombination band at 4367 Å, which is much weaker than the nearby $A\Omega' = 2.5$–$X\Omega'' = 2.5$ (1, 0) and (0, 0) bands, has enabled us to link all of the known states of PtH. The corresponding $\Omega' = 1.5$–$X\Omega'' = 2.5$ (0, 0) intercombination band of PtD at 4358 Å has also been observed at high resolution. Two other weak bands of PtH, located at 4358 and 4695 Å, have been observed in low-resolution scans and are now being analyzed.

Two bands of PtH, whose band origins lie at 11 935 and 11 867 Å, and are assigned as $\Omega' = 1.5$–$X\Omega'' = 1.5$ (0, 0) and (1, 1) bands, respectively, have been observed by Fourier transform infrared emission spectroscopy. Identical transitions occur in PtD at 11 941 and 11 893 Å. The $\Omega' = 1.5$ upper state in all of these transitions appears to be the state of $^2\Pi_{3/2}$ parentage which is predicted by ab initio calculations (*11*) to lie at 10 850 cm^{-1}. In PtD, a perturbation between $v = 0$ of the $X\Omega = 1.5$ lower state and $v = 2$ of the $X\Omega = 2.5$ ground state allowed an independent derivation of the $X\Omega = 1.5$–$X\Omega = 2.5$ interval.

II. EXPERIMENTAL METHODS

A. Laser Excitation Spectroscopy

Laser excitation spectra of PtH were recorded using a modified version of the hollow cathode sputter source developed by Trkula, Harris, and Hilborn (*12*). In our version of the hollow cathode sputter source a 9:1 Ar/H_2 (or Ar/D_2) gas mixture flows through a small hole in the center of a hollowed-out, grounded, 9-mm-diameter metal cathode. Since high purity Pt metal is very expensive, instead of using a solid Pt metal cathode, we covered the top of an ordinary copper cathode with several sheets of 0.1-mm-thick Pt foil. By sustaining an 80-mA-dc discharge between the cathode and a wire, the tip of which is placed 1 cm above the Pt cathode, PtH molecules are produced. The PtH molecules are entrained by the argon gas, and flow vertically through a 3 mm × 20 mm slit into a second, pumped chamber maintained at ~1.5 Torr. A cw laser beam, collimated to 2 mm in diameter interacts with the PtH molecules 1 cm above the slit after horizontally passing through a window cut at Brewster's angle. PtH molecular

fluorescence excited by the laser via the (v', 0) band is collected in two mutually perpendicular directions either by focusing the fluorescence image by a three lens system onto a side-on photomultiplier tube (PMT, Hamamatsu R928) or by dispersing the fluorescence through a 1 m monochromator (Spex 1802, 1200 grooves/mm, blazed at 12 000 Å, operated in second order). A colored glass filter, appropriately chosen to detect (v', 1) fluorescence and block laser scatter, was also used in conjunction with the side-on PMT (*13*).

Initial, low resolution scans were performed over the entire gain curve of Stilbene 420 laser dye using a 3 W UV-pumped cw standing wave dye laser (Coherent 599-21) to identify PtH bands. By removing the intracavity etalon assembly, tunable laser light between 4200 and 4700 Å, with a linewidth of ~ 1 cm^{-1} and peak power of 250 mW, was obtained. High-resolution (~ 2 MHz linewidth) scans were then performed using a 6 W UV-pumped scanning ring dye laser (Coherent 699-29) operated with Stilbene 420 dye. Single-mode scans were performed in the 4235–4465 Å wavelength region with a laser power of typically 150 mW. In both sets of scans, the cw laser beam was mechanically chopped at 600 Hz and the fluorescence signal demodulated by a lock-in amplifier (Stanford Research Systems SR510) with a time constant of 100 msec. In addition to recording the PtH fluorescence signal, the ring dye laser computer also simultaneously monitored its own internal frequency etalon to detect possible scan discontinuities and recorded the Te_2 absorption spectrum so as to provide an absolute frequency calibration of ± 0.01 cm^{-1} (*14*).

B. Fourier Transform Infrared Emission Spectroscopy

PtH emission spectra were observed using a hollow cathode lamp which has been described previously (*15*). Electronically excited PtH molecules are produced in the source by maintaining a 300-mA-dc discharge between an anode and a Pt cathode in the presence of neon carrier gas (1.6 Torr) and a trace amount of hydrogen gas (0.02 Torr). Emission spectra of PtD were obtained under similar conditions using deuterium instead of hydrogen gas. The spectra obtained under these conditions also include emission spectra of other species, such as the earlier analyzed forbidden lines of atomic platinum (*16*).

The emission spectra were recorded with the McMath 1-m Fourier transform spectrometer located at Kitt Peak and operated by the National Solar Observatory. For these measurements the spectrometer (*17*) was operated with CaF_2 beamsplitters and InSb detectors. A total of eight scans of the interferometer were coadded over a period of approximately 1 hr to produce the final interferograms. The spectral bandpass was 1700–9300 cm^{-1} with an instrumental resolution of 0.02 cm^{-1}; the upper and lower limits of the bandpass being set by a Si filter and by the InSb detectors, respectively. The spectra were calibrated using strong neon emission lines (*18*) and are accurate in absolute frequency to ± 0.001 cm^{-1}.

From the intensity patterns of the rotational branches, the rotational temperature of PtH was determined to be about 1200 K and corresponds to a calculated Doppler width of 0.015 cm^{-1}. The narrowest PtH lines are about 0.025 cm^{-1} wide, which is consistent with the combined effects of both Doppler and instrumental line broadening. The linewidths of PtH lines are approximately the same as the linewidths of known, unblended atomic lines of Pt I in this region.

III. RESULTS

A. Laser Excitation Spectra

Very strong laser excitation spectra of PtH were observed in a low-resolution scan of the 4200–4700 Å region. A portion of that excitation spectrum is shown in Fig. 1. Although the red-degraded $A\Omega' = 2.5\text{–}X\Omega'' = 2.5$ (1, 0) and $A\Omega' = 2.5\text{–}X\Omega'' = 2.5$ (0, 0) bands previously observed by Scullman are the most prominent features, we were able to identify without difficulty another band, with its bandhead at 4367 Å, which is located equidistant between the $A\text{–}X$ (1, 0) and (0, 0) band systems. Another weak PtH band with its bandhead at 4387 Å, which has not yet been assigned, can also be seen just to the red of the 4367 Å band. Finally, to the blue of the $A\text{–}X$ (1, 0) band, high-J lines of the $\Omega' = 3.5\text{–}X\Omega'' = 2.5$ (0, 0) transition can be seen. We followed the initial, low-resolution scans with high-resolution scans in the 23 600–22 400 cm^{-1} region. Due to the low power of Stilbene 420 in our 699-29 dye laser, we were unable to scan the entire dye gain curve region in single-mode operation. However, despite these experimental limitations, both the 4367 Å band of PtH and the 4358 Å band of PtD have been fully rotationally analyzed. High-resolution scans and a complete rotational analysis have not yet been performed on the 4387 Å PtH band identified in the low-resolution survey spectra.

The laser excitation spectra of PtH give some of the most intense molecular fluorescence so far observed in any transition metal hydride, including NiH. Fluorescence from both the strong $A\text{–}X$ (1, 0) and (0, 0) bands and the 4367 Å band is easily visible by eye and occurs not only in the region of the 3 mm × 20 mm slit nozzle, but along the laser axis for the entire 30 cm length of the sputter source chamber. For other transition metal hydrides, like FeH, CoH, MnH, and NiH, laser excited molecular

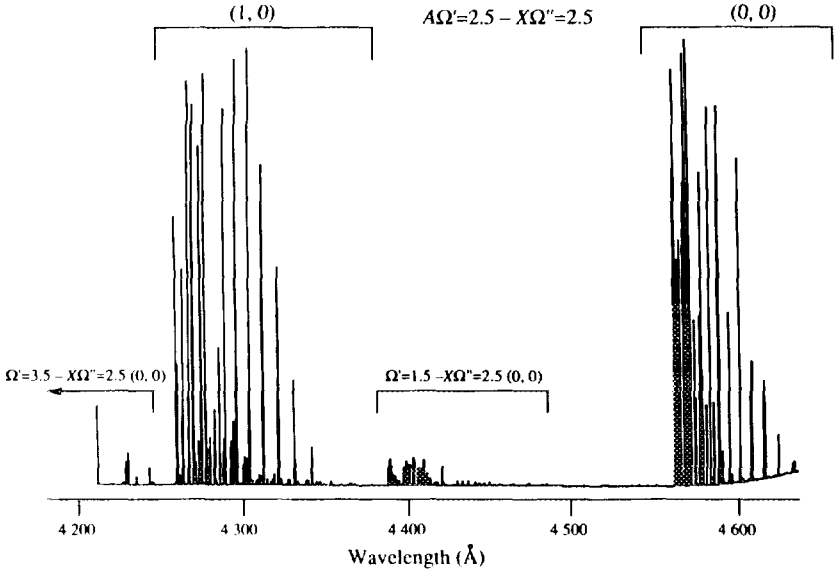

FIG. 1. Laser excitation spectrum of gas-phase PtH in the 4200–4700 Å wavelength region using a Coherent 599-21 laser operated in broadband mode (~1 cm^{-1} linewidth). In addition to the previously observed $\Omega' = 3.5\text{–}X\Omega'' = 2.5$ (0, 0) and $A\Omega' = 2.5\text{–}X\Omega'' = 2.5$ (1, 0) and (0, 0) bands, two additional, weak PtH transitions can be seen.

fluorescence, viewed by eye, varies from very weak to very strong, but is rarely observed outside the slit nozzle jet region (2 cm in length). The unusual chemical stability of PtH probably can be attributed to its M–H bond strength. Of all of the transition metal–H bonds which have been measured the Pt–H bond is the strongest (*19, 20*), D_e(Pt–H) = 3.11 eV (*11*).

Due to the strong spin-orbit and rotational mixing of the electronic states of PtH, we have chosen to use a modified version of the notation first proposed by Linton *et al.* (*21*) in naming the Hund's case (c) PtH states: $[T_0]\Omega\,(v)$ where T_0 is the energy of the $v = 0$ electronic state in thousands of wavenumbers and v is the vibrational quantum number of the vibronic state in question. Using this notation the "$A^2\Delta_{5/2}$" $v = 1$ state at $T \sim 23\,500$ cm^{-1} ($T_0 \sim 22\,000$ cm^{-1}) is referred to as $A[22.0]2.5\,(1)$. For electronic states where the vibrational numbering is unknown or uncertain the (v) label is either omitted or denoted (?) and T replaces T_0 in the bracket. The advantage of this notation is that it removes the ambiguity of labeling *each* vibronic state as a separate state (with its own unique electronic state label) by explicitly incorporating vibrational information into the electronic state designation. Using this notation we can distinguish electronic states which have different $[T_0]\Omega$'s and relate electronic states which have the same $[T_0]\Omega$ but different amounts of vibrational excitation.

(i) The 4367 Å [$\Omega' = 1.5$–$X\Omega'' = 2.5$ (0, 0)] band of PtH. Using the ground state $X\,2.5\,(0)$ combination differences of Scullman (*1*) and the Lagerqvist method (*22*), rotational analysis of the 4367 Å band, even with low-resolution data, was straightforward. Shown in Fig. 2 is the laser excitation spectrum of the 4367 Å band recorded with a broadband laser (~1 cm^{-1} linewidth). The rotational lines assigned in the 4367 Å band are listed in Table I. To be completely sure that the rotational assignments

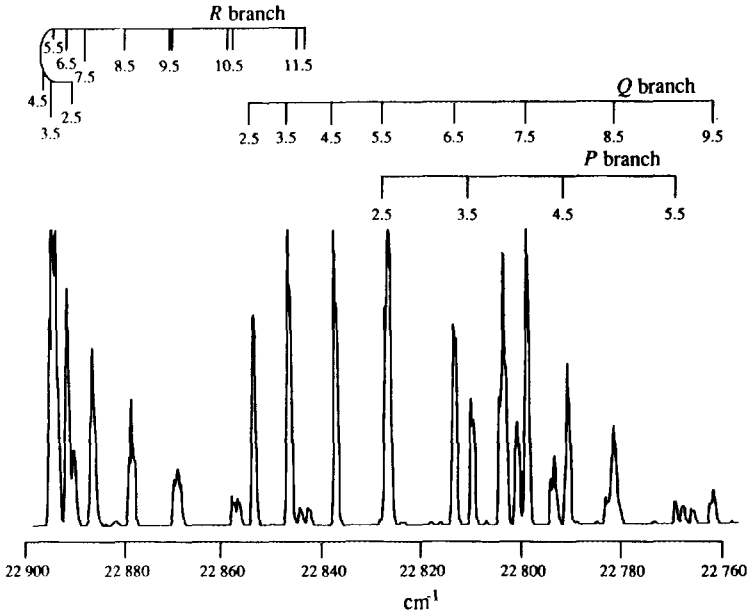

FIG. 2. Laser excitation spectrum of the 4367 Å band [$\Omega' = 1.5$–$X\Omega'' = 2.5$ (0, 0)]. Although weak relative to the strong A–X (1, 0) and (0, 0) band systems, the 4367 Å band could be observed without difficulty. Line assignments are given and another band (head at 4387 Å ~ 22 805 cm^{-1}), is also evident in this wavelength region.

TABLE I

Assigned lines in the 4386 Å Band of PtH [$\Omega' = 1.5\text{–}X\,\Omega = 2.5$ (0, 0)]; Values in cm^{-1}

J''	R_{ee}	R_{ff}	Q_{ef}	Q_{fe}	P_{ee}	P_{ff}
2.5	22 895.68 (0)	22 895.73*	22 853.97 (0)		22 824.13 (- 1)	
3.5	22 899.61 (1)	22 899.69 (2)	22 846.04*	22 846.07*	22 804.31 (- 1)	
4.5	22 901.15 (0)	22 901.29 (0)	22 835.80 (0)	22 835.88 (0)	22 782.22*	22 782.26*
5.5	22 900.31 (0)	22 900.55 (2)	22 823.24 (0)	22 823.37 (0)	22 757.87 (- 1)	22 757.95 (0)
6.5	22 897.01 (0)	22 897.39 (3)	22 808.29 (- 1)	22 808.54 (2)	22 731.22 (- 1)	22 731.36 (0)
7.5	22 891.22 (- 1)	22 891.77 (2)	22 790.95 (- 1)	22 791.33 (2)		
8.5	22 882.88 (- 1)	22 883.66 (1)	22 771.18 (0)	22 771.72 (1)		
9.5	22 871.94 (0)	22 873.02 (1)	22 748.88 (- 2)	22 749.68 (2)		
10.5	22 858.30 (- 1)	22 859.78 (0)	22 724.06 (- 1)	22 725.14 (1)		
11.5	22 841.92 (0)	22 843.88 (- 2)	22 696.60 (- 2)	22 698.09 (1)		

* Blended lines are indicated by an asterisk and were not included in the non-linear least squares fit described in section IV. The values given in parentheses are observed - calculated residuals from this fit.

were correct, dispersed fluorescence experiments were performed on several, individual rotational lines to check that they possessed common upper state rotational levels and that the observed separation between $P(J+1)$–$R(J-1)$ fluorescence lines matched the appropriate ground state combination differences. The first line of the P branch, $P(2.5)$, was clearly resolved in the high-resolution scans and proved that the transition can be unambiguously assigned as $\Omega' = 1.5\text{–}X\,\Omega'' = 2.5$.

We have assigned the $\Omega' = 1.5\text{–}X\,\Omega'' = 2.5$ band at 4367 Å up to $J' = 11.5$ so far. Although lines in the P branch are weak, combination differences [both $\Delta_1 F'$ and $\Delta_2 F'$ (*23*)] show detectable Ω-doubling in the upper state, beginning at $J' = 3.5$. For the ground state, the $\Delta_1 F''$ combination differences do not show any evidence of Ω-doubling, to within our experimental precision, up to $J'' = 11.5$.

The upper state vibrational assignment is deduced to be $v' = 0$ from two observations. First, a similar $\Omega' = 1.5\text{–}X\,\Omega'' = 2.5$ band was observed at nearly the same wavelength in PtD at 4358 Å. Since the excited state vibrational constants of PtH and PtD are quite different ($\sim$2100 and $\sim$1600 cm^{-1}) and both transitions originate from the $X2.5$ (0) state in PtH and PtD, corresponding bands of PtH and PtD can only occur at the same wavelength if $v' = 0$ for both transitions. Second, no isotope splitting was observed at Doppler-limited resolution for any of the lines in the 4367 Å band due to the six naturally occurring isotopes of platinum: ^{190}Pt (0.0127%), ^{192}Pt (0.78%), ^{194}Pt (32.9%), ^{195}Pt (33.8%), ^{196}Pt (25.3%), and ^{198}Pt (7.21%) (*24*). In the very strong $A\Omega' = 2.5\text{–}X\,\Omega'' = 2.5$ (1, 0) band the isotope splitting (^{194}PtH–^{196}PtH or ^{196}PtH–^{198}PtH) is resolvable and is about 1500 MHz.

Although no isotope splitting was observed in the 4367 Å band, two magnetic hyperfine transitions of the form $\Delta F = \Delta J$ were observed at Doppler-limited resolution for every line of the 4367 Å band (see Fig. 3) and result from the $I = \frac{1}{2}$ nuclear spin ($\mu = 0.602$ nucl. magn.) of the ^{195}Pt isotope. The splittings between the two $\Delta F = \Delta J$ hyperfine transitions within each branch are approximately J-independent and are about 2500–3000 MHz. For all three branches the hyperfine widths are approximately equal for lines having the same J'' as well as for lines having the same J'. This means that the hyperfine splittings in both states are similar in magnitude. Using this information and the intensities of the two hyperfine transitions of the $P(2.5)$ line in Fig. 3 we can determine the ordering of the F components and the sign of the hyperfine parameter for both the upper and lower states involved in this transition. From Fig. 3 we see that the stronger $\Delta F = \Delta J$ transition lies to the red of the weaker transition. By making the correspondence that for the $P(2.5)$ line the more intense hyperfine

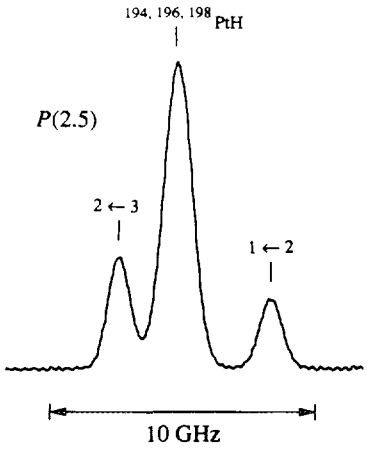

FIG. 3. Laser excitation of the $P(2.5)$ line in the 4367 Å PtH band. Higher energy is to the right and the strong, central feature is due to all of the Pt isotopes, except ^{195}Pt. The $I = \frac{1}{2}$ nuclear spin of the ^{195}Pt isotope causes hyperfine splittings in both the upper and lower states and is responsible for the two weaker features, which are the hyperfine transitions $F' = 2 \leftarrow F'' = 3$ and $F' = 1 \leftarrow F'' = 2$. The 1:3 intensity ratio between the sum of the intensities of the two weaker features and that of the strong feature is consistent with the 33.8% natural abundance of the ^{195}Pt isotope. Also, the relative intensities of the two hyperfine transitions (1.66:1.00) are in satisfactory agreement with the calculated case (a_β) intensities (1.56:1.00) considering that the hyperfine transition $F' = 2 \leftarrow F'' = 3$ is not completely resolved from the central component of the line.

component is the $F' = 2 \leftarrow F'' = 3$ transition, and the weaker component is the $F' = 1 \leftarrow F'' = 2$ transition from case (a_β) coupling transition intensities (*24*) (which will be valid only at low-J), and knowing that the hyperfine splitting is similar in both states, we can conclude that for the $X2.5$ ground state the $F = J + I$ component lies higher in energy than the $F = J - I$ component, while in the [22.8]1.5 (0) state the ordering of the F components is exactly reversed, with the $F = J - I$ component lying above the $F = J + I$ component.

Since no $\Delta F \neq \Delta J$ transitions were observed, it is not possible to determine the absolute frequency separation between the hyperfine components in either the excited or ground state. However, from the information which we do have, we would expect the weaker $\Delta F \neq \Delta J$ transitions to be located somewhere in between the two $\Delta F = \Delta J$ transitions. It is very likely that these weaker transitions are obscured by the strong ^{194}PtH, ^{196}PtH, and ^{198}PtH transitions which also occur in this frequency region. A more complete discussion of the hyperfine interactions is presented later in this section.

The ability to access an $\Omega' = 1.5$ state from the $X2.5$ ground state has allowed us to directly measure the ground state spin–orbit interval between the $X\Omega = 1.5$ and $X\Omega = 2.5$ components by dispersing the laser-induced fluorescence. Also, this intercombination band enables us to determine the absolute energy separation between all of the known PtH electronic states. A typical dispersed fluorescence spectrum is shown in Fig. 4 when the $R(2.5)$ line of the $\Omega' = 1.5$–$X\Omega'' = 2.5$ transition is excited for both PtH and PtD. In the case of PtH, the fluorescence spectrum includes three features at 5090, 5720, and 6498 Å. The molecular fluorescence excited by the purple-colored laser is easily visible by eye since it is a distinct, intense green color. This fluorescence pattern is identical to the emission spectrum for the transition $\Omega' = 1.5$–$X\Omega'' = 1.5$ previously analyzed by Scullman (*2*). It appears that the upper state of both transitions

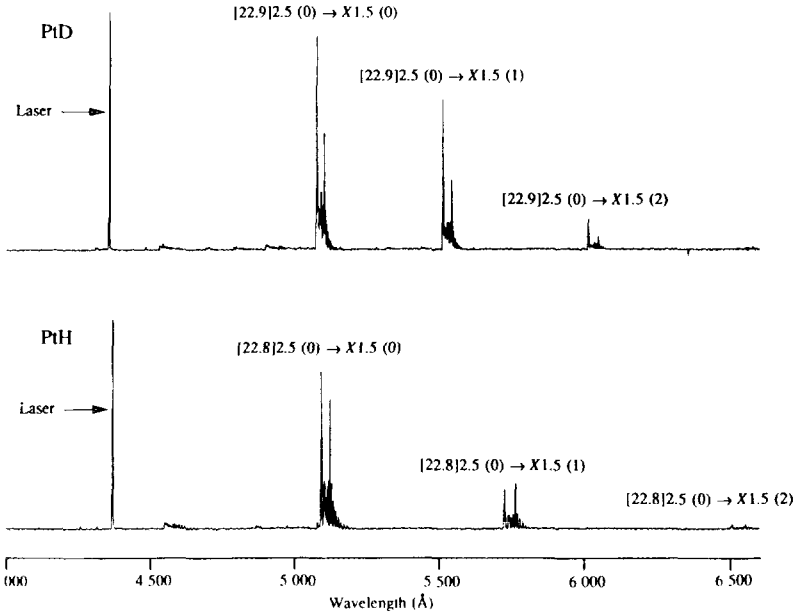

FIG. 4. Dispersed fluorescence spectrum of the $\Omega' = 1.5\text{–}X\,\Omega'' = 2.5$ (0, 0) transition for both PtH and PtD. In both cases, a single-mode cw dye laser (2 MHz linewidth) excited the $R(2.5)$ line and dispersed fluorescence was detected through 300-μm slits. For PtH, three fluorescence features, corresponding to the vibrational progression $\Omega' = 1.5\,(0) \rightarrow X\,\Omega'' = 1.5\,(0), (1)$, and (2) were observed at 5090, 5720, and 6498 Å, respectively. For PtD, three fluorescence features, corresponding to the vibrational progression $\Omega' = 1.5\,(0) \rightarrow X\,\Omega'' = 1.5\,(0), (1)$, and (2) were observed at 5071, 5510, and 6014 Å. Although no other fluorescence features were observed in this wavelength region, the $\Omega' = 1.5$ upper state should also fluoresce in the near-infrared to the low-lying [11.6]1.5 state.

is the same, and that our fluorescence spectrum corresponds to the vibrational progression $\Omega' = 1.5\,(0) \rightarrow X\,\Omega = 1.5\,(v'' = 0, 1,$ and 2). Further evidence in support of this conclusion is that our $\Omega' = 1.5$ upper state rotational constant and combination differences are in excellent agreement with the values for Scullman's $\Omega' = 1.5$ state.

(ii) The 4358 Å [$\Omega' = 1.5\text{–}X\Omega'' = 2.5$ (0, 0)] band of PtD. The $\Omega' = 1.5\text{–}X\,\Omega'' = 2.5$ (0, 0) transition of PtD, located at 4358 Å, is not obvious in the low-resolution survey scans of the 4200–4700 Å wavelength region because it occurs near the strong $A\Omega' = 2.5\text{–}X\,\Omega'' = 2.5$ (1, 0) band system. Once the 4367 Å intercombination band of PtH was identified and assigned, however, high-resolution scans were conducted at the same wavelength region with PtD to identify the corresponding intercombination band and confirm the vibrational assignment of both bands. Assignment and analysis of the 4358 Å PtD band was relatively easy since lines in this band are reasonably strong and can be easily distinguished from other strong lines [i.e., $A\text{–}X$ (1, 0) lines] in this wavelength region by their distinctive isotope/hyperfine pattern. [All of the lines in the $A\text{–}X$ (1, 0) band have resolvable isotope structure at Doppler-limited resolution.] As was the case for the 4376 Å band of PtH, the first line of the P branch, $P(2.5)$, was clearly resolved at high resolution and confirmed the $\Omega' = 1.5\text{–}X\,\Omega'' = 2.5$ electronic assignment of this band.

The rotational lines assigned in the 4358 Å band of PtD are listed in Table II. We have been able to follow this band up to $J' = 20.5$ and, as in PtH, observed no evidence of Ω-doubling in the $X2.5$ ground state of PtD. The $\Omega' = 1.5$ upper state shows

TABLE II

Rotational Lines Assigned in the 4358 Å Band of PtD [$\Omega' = 1.5\text{-}X\,\Omega = 2.5\ (0, 0)$]; Values in cm^{-1}

J''	R_{ee}	R_{ff}	Q_{ef}	Q_{fe}	P_{ee}, P_{ff}
2.5	22 946.21 (1)		22 925.56 (1)		22 910.79 (0)
3.5	22 947.53 (1)		22 920.98 (0)		22 900.33 (1)
4.5	22 947.53 (0)		22 915.11 (0)		22 888.57 (1)
5.5	22 946.21 (0)		22 907.93 (1)		22 875.49 (- 1)
6.5	22 943.59*		22 899.42 (- 1)		22 861.15 (1)
7.5	22 939.59 (- 1)		22 889.61 (- 1)		22 845.47 (0)
8.5	22 934.27 (- 1)	22 934.30 (0)	22 878.47 (- 1)	22 878.49 (0)	22 828.49 (- 1)
9.5	22 927.61 (0)	22 927.65 (- 1)	22 866.00 (- 2)	22 866.04 (0)	22 810.24 (1)
10.5	22 919.57 (- 4)	22 919.65 (0)	22 852.21 (- 2)	22 852.27 (0)	
11.5	——— [a]	22 910.29 (- 1)	22 837.07 (- 5)	22 837.16 (0)	
12.5	22 899.51 (0)	22 899.58 (- 1)	——— [a]	22 820.71 (0)	
13.5	22 887.40 (- 1)	22 887.50 (0)	22 802.86 (1)	22 802.93 (1)	
14.5	22 873.91 (- 1)	22 877.04 (1)	22 783.68 (- 2)	22 783.79 (0)	
15.5	22 859.02 (- 1)	22 859.18 (0)	22 763.16 (- 2)	22 763.30 (0)	
16.5	22 842.73 (- 1)	22 842.94 (1)	22 741.28 (- 2)	22 741.45 (1)	
17.5	22 825.03 (- 2)	22 825.28 (1)	22 718.01 (- 3)	22 718.23 (1)	
18.5	22 805.91 (- 2)	22 806.20 (0)			
19.5	22 785.35 (- 3)	22 785.69 (- 1)			

* Blended lines are indicated by an asterisk and were not included in the non-linear least squares fit described in section IV. The values given in parentheses are observed - calculated residuals from this fit.

[a] line not found.

resolvable Ω-doubling beginning at $J' = 8.5$. However, unlike in the PtH intercombination band, in this band there appears to be a small perturbation in the e parity levels at $J' = 12.5$. This perturbation is the reason that we have been unable to locate the $R_{ee}(11.5)$ and $Q_{ef}(12.5)$ transitions and why both the $R_{ee}(10.5)$ and $Q_{ef}(11.5)$ lines are slightly displaced from their predicted positions. Another clue suggesting that the $J' = 11.5$ and $J' = 12.5$ levels are perturbed is the small, but discernible, irregular size of the upper state Ω-doubling observed between $J' = 10.5$ and $J' = 12.5$. Although we can say very little about the nature of the perturbation, since only the e parity levels in the $\Omega' = 1.5$ state are affected by the perturber, the perturbing state, possibly an $\Omega = 0.5$ state, must, in all likelihood, have a very large Ω-doubling. The reason for this claim is that otherwise we would expect both parity components to be affected by the perturber in the range of rotational levels studied. We are now in the process of conducting a careful search in this wavelength region to find additional, unassigned lines. Finally, the electronic isotope shift between the two $\Omega' = 1.5\text{-}X\,2.5$ bands of PtH and PtD is observed to be about $-80\ cm^{-1}$ ($T_{PtH}-T_{PtD}$).

Although lines in this band and in other PtD bands are reasonably strong, they are typically a factor of three to five times weaker than the same lines in the corresponding PtH bands. Part of this intensity decrease can be explained by the Boltzmann distribution which dilutes the rotational population over a larger number of rotational levels in PtD relative to PtH ($B_{PtH} \sim 2B_{PtD}$). It is also possible that the intensity decrease may be related to the reaction mechanism for the production of transition metal hydrides which would appear, based on our observations, to favor the lighter, more energetic H_2.

(iii) The 4247 Å [$A\Omega' = 2.5\text{-}X\Omega'' = 2.5\ (1, 0)$] band of PtH. We have also re-examined the $A\Omega' = 2.5\text{-}X\,\Omega'' = 2.5$ (1, 0) band of PtH (bandhead at 4247 Å). Like the 4367 Å band, in this band hyperfine structure due to the ^{195}Pt nuclear spin was evident in all of the observed lines. The hyperfine structure, which is resolvable at Doppler-limited resolution, is much larger in the P branch than in the R branch for the same value of J'', but is only slightly larger in the P branch compared to the R

branch for the same value of J'. The J', J'' dependence of the hyperfine structure implies that the hyperfine splitting is larger in the upper state than in the lower state (*25*). For the lowest-J lines, in addition to isotope splittings and strong "main" $\Delta F = \Delta J$ transitions, we have observed weaker, "satellite" $\Delta F \neq \Delta J$ transitions. The presence of these satellite transitions allows the upper and lower state hyperfine splittings to be directly measured from the excitation spectrum.

The lowest R, Q and P lines of the 4247 Å band are shown in Fig. 5. For R and P lines, only three hyperfine transitions, corresponding to two strong $\Delta F = \Delta J$ transitions and one weak $\Delta F \neq \Delta J$ transition, are possible. In the case of Q lines, four hyperfine transitions, corresponding to two strong $\Delta F = \Delta J$ transitions and two weak $\Delta F \neq \Delta J$ transitions, can occur. For the $R(2.5)$, $Q(2.5)$, and $P(3.5)$ transitions, three, four,

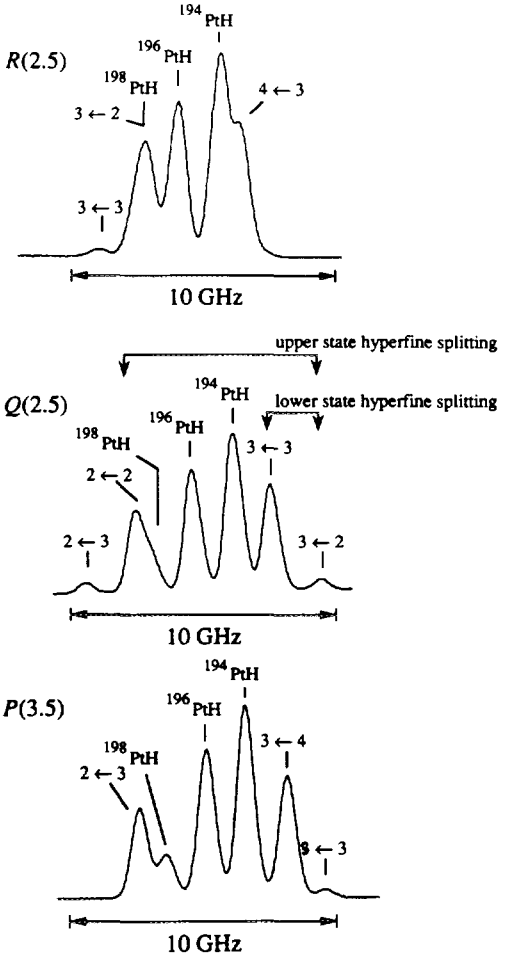

FIG. 5. $R(2.5)$, $Q(2.5)$, and $P(3.5)$ lines of the 4247 Å band [$A\Omega' = 2.5$–$X\Omega'' = 2.5$ (1, 0)] observed in laser excitation. For all three spectra the horizontal scale is identical and higher energy is to the right. For all three lines the isotope splitting is well resolved and is about 1500 MHz between either the ^{198}PtH and ^{196}PtH lines or the ^{196}PtH and ^{194}PtH lines. All hyperfine transitions are denoted $F' \leftarrow F''$. The presence of the weak $\Delta F \neq \Delta J$ transitions provides a direct measure of the absolute hyperfine splitting in both the $A\Omega' = 2.5$ upper and $X\Omega'' = 2.5$ ground states.

and three hyperfine transitions, respectively, were observed. As can be seen from Fig. 5, the hyperfine splitting is much larger in the $A\Omega = 2.5$ (1) excited state than in the $X\Omega = 2.5$ (0) ground state. Also, as we expected from the hyperfine analysis of the 4367 Å band, the hyperfine analysis of this band shows that the ground state hyperfine splitting constant is indeed positive, with the $F = J + I$ component lying higher in energy than $F = J - I$ component. Similarly, for the $A\Omega = 2.5$ (1) upper state, the hyperfine splitting constant is also positive. Splittings were measured at Doppler-limited resolution and are 1850 MHz for $J = 2.5$ and 1350 MHz for $J = 3.5$ of the $X\Omega = 2.5$ (0) ground state; for the $A\Omega = 2.5$ (1) upper state, hyperfine splittings of 6900 and 5300 MHz were measured for $J = 2.5$ and $J = 3.5$, respectively. For J values above $J = 3.5$, all of the weaker $\Delta F \neq \Delta J$ transitions are obscured by the combined effects of Ω-doubling and isotope splittings. At still higher J, where the Ω-doubling is larger than isotope splitting, no satellite transitions are observed.

The reason that the hyperfine splittings in the $A\Omega = 2.5$ upper state are four times larger those of the X 2.5 ground state can probably be related to the increased Pt^+ d^8s character of these states. For all PtH states discussed here, there are two interactions, due to the ^{195}Pt nucleus, which are responsible for the observed molecular magnetic hyperfine effects: Fermi-contact interactions and magnetic dipolar interactions. We can develop a sense of the importance and magnitude of each of these *molecular* terms by examining their *atomic* origin. If one considers PtH to be predominantly ionic Pt^+H^-,[4] then the electronic configurations of the atomic ions which give rise to the ground state of the molecule are Pt^+ d^9 $[^2D]$ and H^- $1s^2$ $[^1S]$. We would expect, then, that the Fermi-contact term (b_F) would contribute nothing to the PtH ground state hyperfine splitting because only molecular states derived from atomic configurations having unpaired s electrons contribute significantly to the Fermi-contact parameter. Although b_F will be negligible for a d^9 configuration, we can estimate the size of the other hyperfine interactions, specifically the magnetic dipole parameter, which gives rise to hyperfine splittings in the ground state of PtH, from ab initio calculations for this atomic-ion parent configuration. For the $5d^9$ electronic configuration of the Pt^+ atomic-ion the magnetic dipole interaction parameter is calculated to be ~900 MHz ($\langle r^{-3} \rangle = 11.29$ a.u.) (*26*).

Unlike the ground state, the excited states of PtH are certainly more d^8s in character because, in the atomic-ion, the d^8s states lie 14 100 cm^{-1} above the d^9 ground state.[5] Molecular states derived from the Pt^+ atomic ion $d^8[^3F]s$ configuration, unlike the low-lying d^9 $[^2D]$ states, should exhibit a very large, positive Fermi-contact interaction due to the nonzero expectation value of the s electron at the nucleus. The ab initio value for the Fermi-contact interaction constant of this configuration has been calculated (*26*) and is $b_F = 13\,967$ MHz. Magnetic dipole interactions due to d electrons will also contribute to the hyperfine splittings in the Pt^+ $5d^86s^1$ electronic configuration as they did in the Pt^+ $5d^9$ configuration. Although neither the magnetic dipole interaction constant nor the expectation value of $\langle r^{-3} \rangle$, which determines the magnitude of the magnetic dipole parameter, has been calculated for this configuration, the size of this term should be similar to the value of the magnetic dipole parameter for both the Pt^+ atomic-ion $5d^9$ ground state configuration (given earlier) and the Pt neutral

[4] The Pt^+H^- ionic approximation is justified in the case of PtH because the ionic–covalent curve crossing is at 1.75 Å, which is some 15% larger than the ground state equilibrium internuclear distance of 1.53 Å.

[5] The energies given are the degeneracy-weighted averages over all the L–S terms terms in the specified configuration.

atom $5d^86s^2$ configuration, where the magnetic dipole parameter is ~983 MHz ($\langle r^{-3} \rangle$ ~ 11.90 a.u.) (*26*).

Consequently, the large difference between the ground and excited state hyperfine splittings in PtH cannot be explained by a large difference in the molecular magnetic dipole parameters of these states, but rather is most likely due to increased Fermi-contact interactions in the excited states. To more fully understand and elucidate both the nature of the bonding in PtH and the atomic configurational parentage of all of the PtH states, sub-Doppler experiments to determine hyperfine parameters will have to be conducted. It is hoped that these experiments can be carried out in the near future.

(iv) Other partially analyzed bands of PtH and PtD. High-resolution scans and a complete rotational analysis have not yet been performed on two weak PtH bands identified in our low-resolution survey spectra. One of the PtH bands, located at 4387 Å, appears strongly perturbed because it has an irregular band structure and because we have been unable to assign rotationally any lines in our low-resolution spectrum using the $R(J-1)$–$Q(J)$–$P(J+1)$ ground state combination differences. The other PtH band, whose head lies at 4695 Å, has been observed at the extreme red end of the Stilbene 420 dye curve and consequently only a few lines in the R branch could be identified. A definitive electronic assignment is not possible since neither the Q-branch nor the P-branch regions were scanned at low-resolution. Since typical excited state vibrational intervals in PtH ($\Delta G_{1/2}$) are 1450–1500 cm^{-1}, it is possible that the 4695 Å band and the 4387 Å band, located some 1500 cm^{-1} higher in energy, may differ by one vibrational quantum. In any case, the excited state of the 4695 Å band is located below the $A[22.0]2.5$ (0) state. High-resolution scans are now under way to analyze rotationally these two remaining weak PtH bands.

B. Fourier Transform Infrared Emission Spectra

Bands of PtH and PtD are not at all obvious in the emission spectrum of the Pt hollow cathode lamp because they are weak and lie within a forest of strong neon lines. The PtH bands were originally overlooked in this spectrum when atomic Pt transitions were previously analyzed. Emission spectra of PtH were first noted

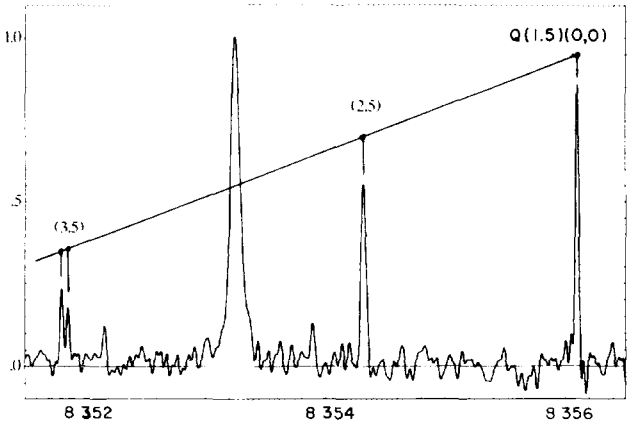

FIG. 6. The Q-branch region of the $\Omega' = 1.5 \rightarrow X\Omega'' = 1.5$ (0, 0) band of PtH. The strong line near 8353.3 cm^{-1} does not belong to PtH.

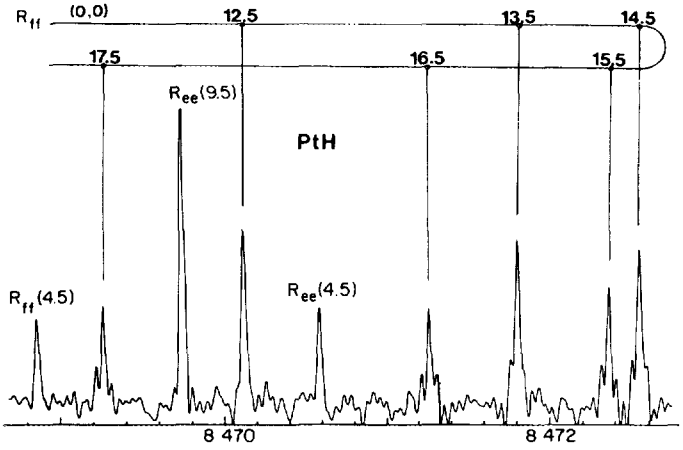

FIG. 7. The region near the R_{ff}-head of the $\Omega' = 1.5 \rightarrow X\,\Omega'' = 1.5$ (0, 0) band of PtH. Note the hyperfine pattern in the high-J lines of the R_{ff} branch.

when the R_{ff}-head in the 11 935 Å band (see Fig. 7) was recognized. Combination differences of this previously unknown doublet band are in agreement with the lower state combination differences derived from the PtH $\Omega' = 1.5$–$X\,\Omega = 1.5$ (0, 0) band of Kaving and Scullman (2). Similar agreement was found between the corresponding PtD combination differences of Gustafsson and Scullman (6) and a doublet band in our Pt/D_2 hollow cathode spectrum. For all four electronic transitions of PtH and PtD, no $P(1.5)$ line was found, forcing us to conclude that the electronic assignment in each case was $\Omega' = 1.5$–$X\,\Omega = 1.5$. Attempts to locate transitions between the predicted $\Omega = 0.5$ states in the near infrared emission spectra were unsuccessful.

A computer code called DECOMP, developed by J. W. Brault of the National Solar Observatory, was used to analyze the Fourier transform data. The line profiles were fit to Voigt functions and linelists were made. Using a least-squares fitting program we were then able to predict and extend branch assignments, and, finally, to determine molecular constants. An accurate, predictive fitting strategy was crucial in detecting the weak PtH emission lines amongst other, stronger emission features.

The $\Omega' = 1.5$ and $X\,\Omega'' = 1.5$ states involved in the infrared electronic transition are far from pure Hund's case (a) $^2\Pi_{3/2}$ and $^2\Delta_{3/2}$ states. Ab initio calculations indicate that the $\Omega' = 1.5$ has 50% $^2\Pi_{3/2}$, while the $X\,1.5$ state has 56% $^2\Delta_{3/2}$ character. Indeed, $^2\Delta_{3/2}$–$^2\Pi_{3/2}$ transitions are forbidden for Hund's case (a) states, but they occur for PtH because of the extensive electronic state mixing caused by the large Pt atomic spin–orbit ζ_{5d} coupling constant. The observed line positions were, therefore, fitted using the simple Hund's case (c) energy level expression described in Section IV.

The rotational lines assigned in the $\Omega' = 1.5$–$X\,\Omega'' = 1.5$ (0, 0) and (1, 1) bands of PtH and PtD are given in Tables III–VI. A careful search for the emission spectra of the $\Omega' = 1.5$–$X\,\Omega'' = 1.5$ (1, 0), (0, 1) and (2, 2) bands of PtH and PtD was not successful. The strongest emission lines, which had a signal-to-noise ratio of about 30, were in the $\Omega' = 1.5$–$X\,\Omega'' = 1.5$ (0, 0) band of PtH around $J = 7.5$. Lines of the other bands were considerably weaker. For all four transitions, the intensity of the Q

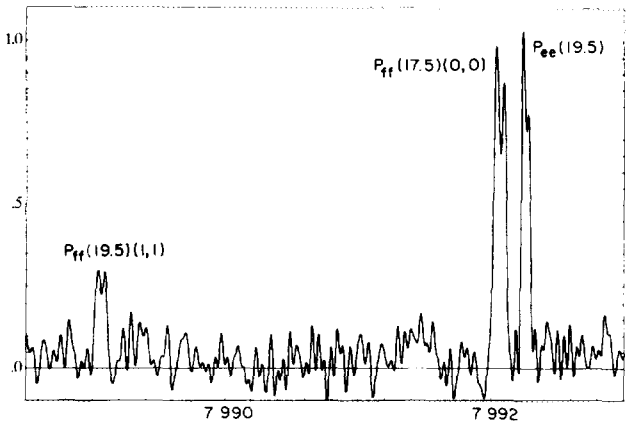

FIG. 8. P-branch lines of the $\Omega' = 1.5 \rightarrow X\,\Omega'' = 1.5$ (0, 0) band of PtH showing isotope splittings. The centers of gravity of these lines were used in our fits.

branch rapidly decreases with increasing J, which is consistent with a $\Delta\Omega = 0$ assignment (Fig. 6).

We have assigned the strongest band, the $\Omega' = 1.5$–$X\,\Omega'' = 1.5$ (0, 0) PtH band at 11 935 Å up to $J' = 26.5$. Combination differences show that the rotational energy levels of both the upper and lower $\Omega = 1.5$ states are Ω-doubled. For both the X 1.5 state and the [11.6] 1.5 state, Ω-doubling is observed for the lowest possible rotational level, $J = 1.5$. The Ω-doubling is slightly smaller in the X 1.5 (0) vibrational level than in the X 1.5 (1) level, but it is slightly larger than in the $v = 0$ vibrational level of the [11.6] 1.5 state. For PtD, Ω-doubling was also observed in both the upper and lower states. Also, for both molecules the Ω-doubling in both the X 1.5 (0) and (1) and the [11.6] 1.5 (0) and (1) sets of states is much larger in size than the Ω-doubling in any of the known excited states located above 22 000 cm^{-1}. Shown in Fig. 6 is the Q branch of the PtH $\Omega' = 1.5$–$X\,\Omega'' = 1.5$ (0, 0) band as it broadens and splits into Q_{ef} and Q_{fe} subbranches.

Like the laser excitation data, some of the PtH emission spectra show evidence of magnetic hyperfine structure due to the ^{195}PtH isotope. Although the resolution of the emission data is only 0.02 cm^{-1} (0.6 GHz), there is some evidence for hyperfine structure in the R branch shown in Fig. 7 for $J'' = 13.5$ through $J'' = 17.5$. This hyperfine splitting pattern is nearly identical to the pattern observed in laser excitation of the $P(2.5)$ line in the 4367 Å band (see Fig. 3). The splitting pattern cannot be due to isotope effects, since they were calculated to be negligible in the R branch. No splittings which could be attributed to hyperfine effects were observed in either the P or Q branches.

Although the P-branch lines do not display any evidence of magnetic hyperfine structure, they display a different splitting pattern than the R-branch lines. Figure 8 shows a section of the PtH $\Omega' = 1.5$–$X\,\Omega'' = 1.5$ (0, 0) P-branch where several doublets are seen. Similar splittings were found in the PtH (1, 1) and PtD (0, 0) bands, but in the PtD (1, 1) band, high-J lines were too weak to be measured. The centroids of these doublets are provided in Tables III–V and were used in our fits. It is most likely that this doubling of the P lines is due to isotope splittings, but calculated separations based on the ρ^2 and ρ^4 dependences of B_v and D_v, gave only qualitative agreement

TABLE III

Assigned Lines in the 11 935 Å Band of PtH [$\Omega' = 1.5$–$X\Omega = 1.5$ (0, 0)]; Transition Wavenumbers Are Given in cm^{-1}

J''	R_{ee}	R_{ff}	P_{ee}	P_{ff}
1.5	8 390.265 (- 5)	8 390.115 (3)	———	———
2.5	8 402.240 (- 4)	8 401.825 (3)	8 320.290 (3)	8 320.151 (5)
3.5	8 413.586 (- 3)	8 412.711 (3)	———[a]	8 303.920 (3)
4.5	8 424.327 (- 2)	8 422.742 (1)	8 287.737 (- 3)	8 286.912 (5)
5.5	8 434.485 (- 1)	8 431.899 (2)	8 270.620 (- 2)	8 269.105 (3)
6.5	8 444.085 (1)	8 440.156 (0)	8 252.990 (- 1)	8 250.490 (2)
7.5	8 453.145 (1)	8 447.498 (- 2)	8 234.881 (1)	8 231.055 (0)
8.5	8 461.690 (3)	8 453.910 (- 3)	8 216.329 (2)	8 210.793 (- 3)
9.5	8 469.738 (3)	8 459.383 (- 3)	8 197.368 (2)	8 189.705 (- 3)
10.5	8 477.309 (2)	8 463.908 (- 3)	8 178.031 (1)	8 167.788 (- 4)
11.5	8 484.424 (3)	8 467.486 (- 1)	8 158.355 (3)	8 145.048 (- 3)
12.5	8 491.097 (2)	8 470.115 (2)	8 138.366 (1)	8 121.492 (- 3)
13.5	8 497.346 (0)	8 471.799 (4)	8 118.100 (1)	8 097.136 (1)[b]
14.5	8 503.188 (- 2)	8 472.544 (5)	8 097.583 (0)	8 071.995 (7)[b]
15.5	8 508.643 (0)	8 472.359 (2)	8 076.845 (- 2)	8 046.087*
16.5	8 513.719 (- 2)	8 471.260 (0)	8 055.916 (- 4)[b]	8 019.437*
17.5	8 518.436 (- 1)	8 469.259 (- 4)	8 034.829 (1)[b]	7 992.061*
18.5	8 522.806 (0)	8 466.364*	8 013.594 (- 5)[b]	7 964.005*
19.5	8 526.843 (1)	8 462.614 (- 6)	7 992.257 (- 2)[b]	7 935.270 (- 3)[b]
20.5	8 530.557 (- 3)	8 458.002 (5)	7 970.838 (3)[b]	7 905.917 (- 5)[b]
21.5	8 533.977 (3)		7 949.352 (0)[b]	7 875.770*
22.5	8 537.098 (0)		7 927.839 (2)[b]	7 845.439*
23.5	8 539.934*		7 906.319 (4)[b]	7 814.404 (0)[b]
24.5			7 884.810 (- 2)[b]	7 782.854*
25.5			7 863.352 (- 2)[b]	
26.5				
27.5			7 820.674 (2)[b]	

J''	Q_{ef}	Q_{fe}
1.5	8 356.093 (- 3)	8 356.093 (4)
2.5	8 354.328 (1)	8 354.302 (- 1)
3.5	8 351.855 (- 2)	8 351.803 (0)
4.5	8 348.696 (3)	8 348.588 (- 3)
5.5	8 344.833 (- 7)	8 344.664 (- 6)
6.5		8 340.048 (0)[b]

* Blended lines are indicated by an asterisk and were not included in the non-linear least squares fit described in section IV. The values given in parentheses are observed - calculated residuals from this fit.

[a] no measurement possible due to blending with a strong atomic line.

[b] mean value of doublet given.

with the observed splittings. Lines in neither the R nor the Q branch showed any doubling at high J.

IV. ANALYSIS OF THE SPECTRUM

A. Calculation of Molecular Constants

We have chosen to fit all of the observed line positions of both PtH and PtD to a simple Hund's case (c) energy level expression (*27*), including parity, of the form

$$E(J) = T_0 + \Delta G_{1/2} + B_v[J(J+1) - \Omega^2] - D_v[J(J+1) - \Omega^2]^2 + H_v[J(J+1) - \Omega^2]^3 + L_v[J(J+1) - \Omega^2]^4 \pm \sum_{n=0}^{n=4} p_{2n+1}(J+0.5)^{2n+1}. \quad (1)$$

The Ω-doubling terms (for $\Omega \geq \frac{3}{2}$) are of the form $\pm p_{2\Omega-2}(J+0.5)^{2\Omega-2}$, $\pm p_{2\Omega}(J+0.5)^{2\Omega}$, $\pm p_{2\Omega+2}(J+0.5)^{2\Omega+2}$, $\pm p_{2\Omega+4}(J+0.5)^{2\Omega+4}$, etc., since we expect the Ω-doubling

TABLE IV

Assigned Lines in the 11 867 Å Band of PtH [$\Omega' = 1.5\text{-}X\,\Omega = 1.5$ (1, 1)]; Transition Wavenumbers Are Given in cm^{-1}.

J''	R_{ee}	R_{ff}	P_{ee}	P_{ff}
1.5	8 437.814 (- 2)	8 437.646 (- 3)	———	———
2.5	8 449.358 (- 1)	8 448.903 (- 1)	8 369.886 (- 5)	———[a]
3.5	8 460.271 (0)	8 459.319 (3)	8 354.392 (1)	8 353.885 (0)
4.5	8 470.581 (1)	8 468.859 (3)	8 338.119 (- 2)	8 337.581 (2)
5.5	———[a]	8 477.498 (- 3)	8 321.391 (1)	8 319.755 (0)
6.5	8 489.487 (2)	8 485.228 (0)	8 304.150 (2)	8 301.755 (0)
7.5	8 498.129 (- 1)	8 492.018 (- 4)	8 286.432 (1)	8 282.314 (3)
8.5	8 506.266 (1)	8 497.870 (2)	8 268.277 (0)	8 262.321 (- 1)
9.5	8 513.914 (0)	8 502.759 (- 1)	8 249.724 (3)	8 241.485 (0)
10.5	8 521.095 (0)	8 506.700*	8 230.799 (0)	8 219.797 (- 5)
11.5	8 527.830 (1)	8 509.667 (1)	8 211.542 (- 2)	8 197.280 (0)[b]
12.5	8 534.133 (- 1)	8 511.685 (1)	8 191.989 (0)	8 173.927 (- 3)[b]
13.5	8 540.026 (- 2)	8 512.753 (- 2)	8 172.164 (- 2)	8 149.767 (- 2)[b]
14.5	8 545.532 (2)	8 512.889 (1)	8 152.107 (1)	8 124.822 (6)[b]
15.5	8 550.567*	———[a]	8 131.842 (1)[b]	8 099.096 (2)[b]
16.5		8 510.383 (- 1)	8 111.388*	8 072.635 (5)[b]
17.5		8 507.802*	8 090.914*	8 045.443 (- 9)[b]
18.5	8 563.976*		———[a]	———[a]
19.5		8 499.977*	———[a]	7 989.062 (2)[b]
20.5			8 028.532 (0)[b]	

J''	Q_{ef}	Q_{fe}
1.5	8 404.679 (1)	8 404.679 (4)
2.5	8 402.885 (1)	8 402.854*

* Blended lines are indicated by an asterisk and were not included in the non-linear least squares fit described in section IV. The values given in parentheses are observed - calculated residuals from this fit.

[a] no measurement possible due to blending with a strong atomic line.

[b] mean value of doublet given.

to be approximately proportional to $J^{2\Omega}$ and its higher-order terms (*28, 29*). In addition, we have made *e/f* parity assignments for all the $\Omega = 1.5$ states based on the assumption that a single $\Omega = 0.5$ state ($^2\Sigma^+$ and $^2\Pi_{1/2}$ mixture) lies between the $X\,2.5$ and $X\,1.5$ ground state components. Our placement of the $\Omega = 0.5$ state is consistent with ab initio calculations (*11*) which place this state 1500 cm^{-1} above the $X\,2.5$ state. By assuming that the *f*-parity levels lie above the *e*-parity levels in the $X\,1.5$ state, we can then unambiguously determine the *e/f* parity of all the states which are either directly or indirectly connected to the $X\,1.5$ state. If our assumption of the absolute sign of the Ω-doubling in the $X\,1.5$ state is incorrect, although the absolute parity labels of all the states will need to be reversed, we are still guaranteed that all the relative parity assignments have been made correctly.

We have performed a nonlinear least-squares fit using all of the available laser excitation, Fourier transform, and previous absorption and emission data for the known electronic states of PtH and PtD below 3 eV. In the PtH fit, 660 rotational lines were fit and 64 parameters were varied; in the PtD fit, 782 transitions were input and 47 molecular constants were varied. In both fits the uncertainties in the data sets are: laser excitation data ± 0.01 cm^{-1}, Fourier transform data ± 0.001 cm^{-1}, and previous absorption and emission data ± 0.07 cm^{-1} (low-J Ω-doubled lines were de-weighted to ±0.15 cm^{-1}). For PtD, in the $\Omega' = 1.5\text{-}X\,\Omega'' = 1.5$ (0, 0) transition, low-J lines were found to be displaced from their expected positions and these perturbed lines were not used in the fits. The PtD (1, 1) infrared emission band was quite weak and relatively few lines of reduced accuracy (±0.006 cm^{-1}) were found. The variance in

TABLE V

Rotational Lines Assigned in the 11 941 Å Band of PtD [$\Omega' = 1.5\text{–}X\,\Omega = 1.5\ (0, 0)$]; Transition Wavenumbers Are Given in cm^{-1}

J''	R_{ee}	R_{ff}	P_{ee}	P_{ff}
1.5	8 381.160 (- 9)	8 381.160 (15)	———	———
2.5	8 387.768 (1)	8 387.701 (- 5)	———[a]	———[a]
3.5	8 394.224 (8)[c]	8 394.097 (6)[c]	8 338.392 (5)[c]	8 338.337 (5)*
4.5	8 400.529 (11)[c]	8 400.310 (16)[c]	8 330.756 (10)[c]	8 330.654 (23)[c]
5.5	8 406.732 (55)[c]	8 406.394*	8 323.031 (58)[c]	8 322.832 (68)[c]
6.5	8 412.657 (- 36)[c]	8 412.113 (- 24)[c]	8 315.041 (- 32)[c]	8 314.701 (- 27)[c]
7.5	8 418.557 (- 12)[c]	8 417.755 (- 11)[c]	8 307.034 (- 18)[c]	8 306.511 (- 12)[c]
8.5	8 424.294 (- 13)[c]	8 423.185 (- 8)[c]	8 298.907 (- 8)[c]	8 298.140 (- 6)[c]
9.5	8 429.902 (- 8)	8 428.411 (- 3)	8 290.663 (- 6)	8 289.589 (- 7)
10.5	8 435.374 (- 6)	8 433.432 (9)	8 282.317 (- 1)	8 280.866 (- 5)
11.5	8 440.715 (- 6)	8 438.215 (- 3)	8 273.865 (- 3)	8 271.968 (- 1)
12.5	8 445.928 (- 2)	8 442.791 (- 1)	8 265.320 (- 4)	8 262.888 (- 1)
13.5	8 451.010 (- 4)	8 447.143 (1)	8 256.690 (- 3)	8 253.632 (3)
14.5	8 455.972 (- 2)	8 451.264 (1)	8 247.973 (- 6)	8 244.194 (4)
15.5	8 460.812 (1)	8 455.150 (- 3)	8 239.188 (0)	8 234.567 (- 1)
16.5	8 465.533 (3)	8 458.806 (- 1)	8 230.325 (- 1)	8 224.769 (4)[b]
17.5	8 470.132 (2)	8 462.220 (- 1)	8 221.407 (10)	8 214.780 (1)[b]
18.5	8 474.623 (7)	8 465.398 (5)	8 212.409 (0)	8 204.612 (2)[b]
19.5	8 479.003*	8 468.330 (10)	8 203.357*	8 194.246*
20.5	8 483.250 (- 1)	8 470.991 (- 9)	8 194.278 (6)[b]	8 183.724 (3)[b]
21.5	8 487.416*	8 473.435*	8 185.137 (3)[b]	8 173.004 (2)[b]
22.5	8 491.449 (- 4)	8 475.606 (0)	8 175.968 (9)[b]	8 162.097 (- 4)[b]
23.5	8 495.282*	8 477.527 (- 2)	8 166.746 (- 4)[b]	8 151.014 (- 4)[b]
24.5	8 499.049*		8 157.515 (1)[b]	8 139.751 (- 4)[b]
25.5	8 502.991 (4)		8 148.238 (- 17)[b]	8 128.310 (- 3)[b]
26.5	8 506.636 (- 1)		8 138.976 (- 5)[b]	8 116.698 (4)[b]
27.5			8 129.702 (6)[b]	8 104.904 (4)[b]
28.5			8 120.409 (3)[b]	8 092.924*

J''	Q_{ef}	Q_{fe}
1.5	8 363.716 (1)	8 363.716 (2)
2.5	8 363.322 (- 3)	8 363.322 (2)
3.5	8 362.780*	8 362.780*
4.5	8 362.070*	8 362.070*

* Blended lines are indicated by an asterisk and were not included in the non-linear least squares fit described in section IV. The values given in parentheses are observed - calculated residuals from this fit.

[a] no measurement possible due to blending with a strong atomic line.

[b] mean value of doublet given.

[c] perturbed lines, not used in least squares fit. See section IV (b) for explanation and discussion.

both the PtH and the PtD fit was 1.1. The T, $\Delta G_{1/2}$, B_v, D_v, H_v, L_v, and p values calculated from Eq. (1), along with a summary of the spectroscopic constants for all the known PtH electronic states is given in Table VII. A similar tabulation of molecular constants and a summary of the electronic states of PtD can be found in Table VIII. Listed in Tables I–VI, in addition to the PtH and PtD transition frequencies, are observed minus calculated transition frequencies from the least squares output. Calculated energy levels for the $X\,2.5\ (0)$ and (1) states and all of the known $\Omega = 1.5$ states are given in Tables IX–XII and Tables XIII–XVI for PtH and PtD, respectively.

The ground state spin–orbit splitting can be determined from a least squares fit of our laser excitation data and Scullman's emission data. Although we could experimentally measure the $X\,\Omega = 1.5\text{–}X\,\Omega = 2.5$ energy separation using dispersed fluorescence, the measurement uncertainty is limited by the monochromator accuracy which is $\pm 1\ cm^{-1}$. From our fit we derive a value of $3253.74\ cm^{-1} \pm 0.10\ cm^{-1}$ for the spin-orbit interval between the $X\,\Omega = 1.5\ (0)$ ($J = 2.5$, e level) and $X\,\Omega = 2.5\ (0)$

TABLE VI

Rotational Lines Assigned in the 11 893 Å Band of PtD [$\Omega' = 1.5 - X\Omega = 1.5$ (1, 1)]; Transition Wavenumbers Are Given in cm^{-1}

J''	R_{ee}	R_{ff}	P_{ee}	P_{ff}
1.5	————	————		
2.5				
3.5				
4.5	8433.376 (4)			
5.5	8439.374*	8438.999 (1)	8357.426*	8357.226 (5)
6.5	8445.264 (- 5)	8444.679 (2)	8349.693 (1)	8349.351*
7.5	8451.010 (2)	8450.157 (4)	————[a]	————[a]
8.5	8456.608 (- 2)	8455.428 (3)	8333.845 (0)	8333.037 (6)
9.5	8462.076 (- 1)	8460.484 (- 2)	8325.754 (1)	8324.618 (1)
10.5	8467.414 (3)	8465.328 (- 4)	8317.559 (3)	8316.027 (3)
11.5	8472.614 (- 1)	8469.958 (0)	8309.257 (- 3)	8307.248 (- 3)
12.5	8477.706*	————[a]	8300.871 (0)	8298.283 (- 11)
13.5	8482.643*	8478.531 (5)	8292.397 (3)	8289.153 (0)
14.5		8482.455 (- 4)	————[a]	8279.827 (1)
15.5		8486.222*	————[a]	8270.320*
16.5			8266.474*	8260.607 (- 3)
17.5			8257.799*	8250.806*
18.5			8248.997*	8240.703*
19.5				8230.325*
20.5			8231.210 (0)	

J''	Q_{ef}	Q_{fe}
1.5	8397.438*	8397.438 *
2.5	8397.043*	8363.043*

* Blended lines are indicated by an asterisk and were not included in the non-linear least squares fit described in section IV. The values given in parentheses are observed - calculated residuals from this fit.

[a] no measurement possible due to blending with a strong atomic line.

TABLE VII

Molecular Constants for All the Analyzed Electronic States of PtH Below 3 eV;[a] All Values Are Given in cm^{-1}

Constant	X2.5 (0)	X2.5 (1)	X1.5 (0)	X1.5 (1)	[11.6]1.5 (0)	[11.6]1.5 (1)	[22.0]2.5 (0)	[22.8]1.5 (0)	[22.8]1.5 (1)	[23.8] 3.5 (0)
T	0.0	2 293.49[b]	3 224.89 (2)	5 401.76[b]	11 581.55 (2)	13 807.01[b]	21 950.73 (2)	22 832.920 (6)	24 332.55[b]	23 830.70 (4)
$\Delta G_{1/2}$	---	2 293.49 (3)	---	2 176.87 (2)	---	2 225.46 (2)	---	---	1 499.63 (4)	---
	---	2 293.93[c]	---	2 176.50[c]	---	---	---	---	1 498.93[c]	---
B_v	7.096 1 (2)	6.896 0 (6)	7.177 48 (4)	6.974 09 (5)	6.821 63 (4)	6.612 89 (7)	5.533 5 (6)	5.971 1 (3)	5.672 (1)	5.591 (2)
	7.096 5 (2)[c]	6.896 9 (1)[c]	7.177 0 (2)[c]	6.974 1 (7)[c]	---	---	5.534[c]	5.966 9 (4)[c]	5.680 (1)[c]	5.595 (2)[c]
$D_v \times 10^4$	2.614 (6)	2.60 (2)	2.799 (1)	2.776 (3)	2.361 (2)	2.229 (6)	4.08 (4)	4.89 (2)	4.8 (1)	3.49 (7)
	2.613 (4)[c]	2.607 (2)[c]	2.748 (3)[c]	2.84 (3)[c]	---	---	3.546[c]	4.717 (8)[c]	6.08 (6)[c]	3.6 (1)[c]
$H_v \times 10^9$	---	---	-3.6 (1)	-8.5 (6)	19.1 (5)	21. (3)	182. (6)	26. (3)	-3.9 (3)	---
$L_v \times 10^{11}$	---	---	---	---	-2.13 (5)	-3.2 (4)	---	---	---	---
$p_1 \times 10^3$	---	---	-1.6 (1)	-1.5 (3)	-1.7 (1)	-3.2 (3)	---	---	---	---
$p_3 \times 10^3$	---	---	2.147 (1)	2.286 (5)	2.608 (2)	2.910 (6)	---	0.276 (4)	0.65 (2)	---
$p_5 \times 10^7$	---	---	-5.67 (2)	-7.4 (3)	-23.39 (6)	-31.1 (4)	50.9 (7)	10.3 (1)	---	---
$p_7 \times 10^{10}$	---	---	---	1.7 (5)	12.29 (7)	20.5 (7)	-93. (3)	---	146. (4)	---
$p_9 \times 10^{12}$	---	---	---	---	---	---	2.2 (4)	---	---	---

[a] The energy level expression given in Eq. (1) was used to derive the rotational constants. Uncertainties (1σ) are given in parentheses and are in the units of the last significant figure.

[b] T value is given by $T = T_0 + \Delta G_{1/2}$.

[c] For comparison purposes two sets of molecular constants are presented. One set is the constants for all the electronic states which we have analyzed or re-analyzed in this work. The second set of constants is for all the states previously analyzed by Scullman and co-workers [see refs. (1) and (2)].

TABLE VIII

Molecular Constants for All the Analyzed Electronic States of PtD below 3 eV;[a] All Values Are Given in cm^{-1}

Constant	$X2.5\ (0)$	$X2.5\ (1)$	$X1.5\ (0)$	$X1.5\ (1)$	$[11.6]1.5\ (0)$	$[11.6]1.5\ (1)$	$[22.0]2.5\ (0)$	$[22.9]1.5\ (0)$	$[22.9]1.5\ (1)$	$[23.9]\ 3.5\ (0)$
T	0.0	1 644.13[b]	3 228.52 (2)	4 790.63[b]	11 592.36 (2)	13 188.12[b]	22 036.03 (3)	22 915.368 (4)	24 012.23[b]	23 830.70 (4)
$\Delta G_{1/2}$	---	1 644.13 (2)	---	1 562.11 (1)	---	1 595.76 (1)	---	---	1 096.86 (3)	---
	---	1 644.32[c]	---	1 561.92[c]	---	---	---	---	1 096.69[c]	---
B_v	3.603 8 (3)	3.531 9 (2)	3.567 51 (4)	3.493 66 (8)	3.489 09 (4)	3.415 69 (5)	2.877 6 (7)	2.952 4 (1)	2.853 6 (2)	5.591 (2)
	3.604 (1)[c]	3.532 (2)[c]	3.566 9 (3)[c]	3.494 3 (4)[c]	---	---	2.879[c]	2.952 0 (3)[c]	2.853 0 (5)[c]	2.818 1 (2)[c]
$D_v \times 10^5$	6.76 (2)	6.71 (3)	6.92 (1)	6.51 (4)	6.80 (1)	6.74 (2)	6.8 (3)	8.76 (2)	9.58 (3)	3.49 (7)
	6.8 (4)[c]	6.8 (3)[c]	6.84 (3)[c]	6.95 (3)[c]	---	---	7.9[c]	8.76 (2)[c]	9.56 (2)[c]	7.82 (3)[c]
$H_v \times 10^9$	---	---	0.45 (7)	-5.4 (7)	1.29 (8)	---	-39. (4)	---	---	---
$p_3 \times 10^4$	---	---	2.764 (2)	2.88 (1)	3.611 (3)	3.91 (3)	---	0.10 (3)	-0.22 (1)	---
$p_5 \times 10^8$	---	---	---	---	-5.41 (2)	-10. (2)	---	1.7 (6)	---	---
$p_7 \times 10^{10}$	---	---	---	---	---	1.3 (5)	---	---	---	---

[a] The energy level expression given in Eq. (1) was used to derive the rotational constants. Uncertainties (1σ) are given in parentheses and are in the units of the last significant figure.

[b] T value is given by $T = T_0 + \Delta G_{1/2}$.

[c] For comparison purposes two sets of molecular constants are presented. One set is the constants for all the electronic states which we have analyzed or re-analyzed in this work. The second set of constants is for all the states previously analyzed by Scullman and co-workers [see refs. (4), (5), and (6)].

($J = 2.5$, e level) ground state components of PtH. For PtD, from a similar fit of our high-resolution laser excitation data and the emission data, we derive an energy level separation of 3242.69 (± 0.10) cm^{-1} between the $X\,\Omega = 1.5\ (0)$ ($J = 2.5$, e level) and

TABLE IX

Calculated Energy Levels for the $X\,2.5\ (0)$ and $X\,2.5\ (1)$ States of PtH in cm^{-1}

J	$X2.5\ (0)$ e,f levels	$X2.5\ (1)$ e,f levels
2.5	17.739	2 310.732
3.5	67.389	2 358.982
4.5	131.188	2 420.981
5.5	209.108	2 496.700
6.5	301.112	2 586.105
7.5	407.162	2 689.155
8.5	527.209	2 805.803
9.5	661.200	2 935.997
10.5	809.076	3 079.676
11.5	970.771	3 236.776
12.5	1 146.213	3 407.225
13.5	1 335.323	3 590.943
14.5	1 538.017	3 787.848
15.5	1 754.203	3 997.847
16.5	1 983.784	4 220.846
17.5	2 226.658	4 456.739
18.5	2 482.713	4 705.419
19.5	2 751.834	4 966.769
20.5	3 033.898	5 240.668
21.5	3 328.778	5 526.987
22.5	3 636.337	5 825.592
23.5	3 956.436	6 136.343
24.5	4 288.926	6 459.092
25.5	4 633.653	6 793.687
26.5	4 990.458	7 139.969
27.5	5 359.174	7 497.770
28.5	5 739.629	7 866.921
29.5	6 131.644	8 247.242
30.5	6 535.034	8 638.550

TABLE X

Calculated Energy Levels for the $X\,1.5\,(0)$ and $X\,1.5\,(1)$ States of PtH in cm^{-1}

J	$X1.5\,(0)$		$X1.5\,(1)$	
	e levels	*f levels*	*e levels*	*f levels*
1.5	3 235.641	3 235.669	5 412.201	5 412.232
2.5	3 271.478	3 271.584	5 447.019	5 447.133
3.5	3 321.603	3 321.865	5 495.716	5 495.996
4.5	3 385.982	3 386.500	5 558.257	5 558.809
5.5	3 464.570	3 465.471	5 634.597	5 635.556
6.5	3 557.320	3 558.753	5 724.689	5 726.212
7.5	3 664.176	3 666.313	5 828.476	5 830.746
8.5	3 785.077	3 788.113	5 945.898	5 949.118
9.5	3 919.954	3 924.104	6 076.885	6 081.283
10.5	4 068.734	4 074.234	6 221.364	6 227.185
11.5	4 231.337	4 238.439	6 379.254	6 386.763
12.5	4 407.676	4 416.651	6 550.470	6 559.947
13.5	4 597.659	4 608.791	6 734.917	6 746.660
14.5	4 801.188	4 814.775	6 932.498	6 946.816
15.5	5 018.158	5 034.511	7 143.105	7 160.321
16.5	5 248.459	5 267.896	7 366.627	7 387.073
17.5	5 491.974	5 514.822	7 602.946	7 626.963
18.5	5 748.581	5 775.172	7 851.936	7 879.871
19.5	6 018.151	6 048.819	8 113.463	8 145.670
20.5	6 300.551	6 335.630	8 387.390	8 424.226
21.5	6 595.641	6 635.461	8 673.569	8 715.394
22.5	6 903.275	6 948.161	8 971.845	9 019.023
23.5	7 223.301	7 273.569	9 282.058	9 334.950
24.5	7 555.561	7 611.517	9 604.036	9 663.006
25.5	7 899.893	7 961.826	9 937.602	10 003.014
26.5	8 256.126	8 324.308	10 282.569	10 354.787
27.5	8 624.086	8 698.766	10 638.741	10 718.130
28.5	9 003.592	9 084.993	11 005.912	11 092.839
29.5	9 394.458	9 482.774	11 383.867	11 478.703
30.5	9 796.491	9 891.882	11 772.382	11 875.501

TABLE XI

Calculated Energy Levels for the $[11.6]1.5\,(0)$ and $[11.6]1.5\,(1)$ States of PtH in cm^{-1}

J	$[11.6]1.5\,(0)$		$[11.6]1.5\,(1)$	
	e levels	*f levels*	*e levels*	*f levels*
1.5	11 591.765	11 591.730	13 816.910	13 816.877
2.5	11 625.911	11 625.781	13 850.017	13 849.881
3.5	11 673.722	11 673.407	13 896.378	13 896.037
4.5	11 735.193	11 734.572	13 955.988	13 955.311
5.5	11 810.311	11 809.240	14 028.837	14 027.665
6.5	11 899.057	11 897.368	14 114.907	14 113.056
7.5	12 001.404	11 998.909	14 214.174	14 211.440
8.5	12 117.320	12 113.813	14 326.606	14 322.767
9.5	12 246.764	12 242.026	14 452.163	14 446.987
10.5	12 389.690	12 383.490	14 590.799	14 584.042
11.5	12 546.041	12 538.145	14 742.459	14 733.877
12.5	12 715.758	12 705.926	14 907.084	14 896.428
13.5	12 898.771	12 886.764	15 084.604	15 071.631
14.5	13 095.005	13 080.586	15 274.946	15 259.415
15.5	13 304.378	13 287.314	15 478.027	15 459.704
16.5	13 526.802	13 506.868	15 693.762	15 672.414
17.5	13 762.179	13 739.157	15 922.056	15 897.457
18.5	14 010.410	13 984.086	16 162.811	16 134.731
19.5	14 271.386	14 241.551	16 415.922	16 384.122
20.5	14 544.993	14 511.440	16 681.281	16 645.506
21.5	14 831.112	14 793.626	16 958.774	16 918.737
22.5	15 129.616	15 087.973	17 248.284	17 203.650
23.5	15 440.373	15 394.327	17 549.688	17 500.056
24.5	15 763.246	15 712.515	17 862.860	17 807.736
25.5	16 098.092	16 042.346	18 187.670	18 126.440
26.5	16 444.760	16 383.602	18 523.985	18 455.876
27.5	16 803.094	16 736.037	18 871.667	18 795.708
28.5	17 172.932	17 099.374	19 230.572	19 145.547
29.5	17 554.101	17 473.297	19 600.555	19 504.945
30.5	17 946.424	17 857.449	19 981.462	19 873.385

TABLE XII

Calculated Energy Levels for the [22.8]1.5 (0) and [22.8]1.5 (1) States of PtH in cm^{-1}

J	[22.8]1.5 (0)		[22.8]1.5 (1)	
	e levels	*f levels*	*e levels*	*f levels*
1.5	22 841.874	22 841.878	24 341.049	24 341.060
2.5	22 871.704	22 871.720	24 369.377	24 369.413
3.5	22 913.422	22 913.460	24 408.989	24 409.073
4.5	22 966.985	22 967.061	24 459.837	24 460.002
5.5	23 032.337	23 032.472	24 521.860	24 522.150
6.5	23 109.410	23 109.634	24 594.982	24 595.453
7.5	23 198.125	23 198.476	24 679.105	24 679.834
8.5	23 298.390	23 298.915	24 774.109	24 775.199
9.5	23 410.101	23 410.860	24 879.848	24 881.444
10.5	23 533.143	23 534.211	24 996.145	24 998.449
11.5	23 667.386	23 668.855	25 122.784	25 126.081
12.5	23 812.692	23 814.673	25 259.504	25 264.197
13.5	23 968.908	23 971.535	25 405.991	25 412.640
14.5	24 135.871	24 139.304	25 561.871	25 571.249
15.5	24 313.404	24 317.834	25 726.696	25 739.855
16.5	24 501.323	24 506.971	25 899.934	25 918.290
17.5	24 699.428	24 706.555	26 080.955	26 106.388
18.5	24 907.511	24 916.417	26 269.018	26 303.992
19.5	25 125.351	25 136.383	26 463.253	26 510.958
20.5	25 352.718	25 366.273	26 662.646	26 727.167
21.5	25 589.369	25 605.901	26 866.014	26 952.531
22.5	25 835.055	25 855.077	27 071.993	27 187.001
23.5	26 089.513	26 113.604	27 279.005	27 430.579
24.5	26 352.472	26 381.285	27 485.239	27 683.334
25.5	26 623.652	26 657.915	27 688.626	27 945.411
26.5	26 902.764	26 943.290	27 886.803	28 217.047
27.5	27 189.509	27 237.203	28 077.088	28 498.589
28.5	27 483.582	27 539.443	28 256.446	28 790.515
29.5	27 784.668	27 849.802	28 421.451	29 093.447
30.5	28 092.446	28 168.068	28 568.250	29 408.181

TABLE XIII

Calculated Energy Levels for the $X2.5$ (0) and $X2.5$ (1) States of PtD in cm^{-1}

J	$X2.5$ (0)	$X2.5$ (1)
	e, f levels	*e, f levels*
2.5	9.009	1 652.962
3.5	34.230	1 677.680
4.5	66.648	1 709.450
5.5	106.254	1 748.266
6.5	153.040	1 794.118
7.5	206.996	1 846.996
8.5	268.109	1 906.888
9.5	336.366	1 973.780
10.5	411.751	2 047.657
11.5	494.247	2 128.502
12.5	583.835	2 216.297
13.5	680.496	2 311.020
14.5	784.206	2 412.652
15.5	894.944	2 521.167
16.5	1 012.682	2 636.542
17.5	1 137.396	2 758.749
18.5	1 269.056	2 887.760
19.5	1 407.632	3 023.546
20.5	1 553.093	3 166.076
21.5	1 705.406	3 315.315
22.5	1 864.534	3 471.230
23.5	2 030.443	3 633.784
24.5	2 203.094	3 802.939
25.5	2 382.447	3 978.656
26.5	2 568.460	4 160.894
27.5	2 761.091	4 349.610
28.5	2 960.295	4 544.760
29.5	3 166.026	4 746.298
30.5	3 378.236	4 954.176

TABLE XIV

Calculated Energy Levels for the $X\,1.5\,(0)$ and $X\,1.5\,(1)$ States of PtD in cm^{-1}

J	$X1.5\,(0)$		$X1.5\,(1)$	
	e levels	*f levels*	*e levels*	*f levels*
1.5	3 233.873	3 233.877	4 795.877	4 795.881
2.5	3 251.702	3 251.717	4 813.337	4 813.353
3.5	3 276.655	3 276.690	4 837.773	4 837.810
4.5	3 308.723	3 308.792	4 869.177	4 869.249
5.5	3 347.898	3 348.017	4 907.541	4 907.665
6.5	3 394.169	3 394.358	4 952.854	4 953.051
7.5	3 447.523	3 447.806	5 005.104	5 005.399
8.5	3 507.946	3 508.349	5 064.278	5 064.697
9.5	3 575.422	3 575.975	5 130.359	5 130.934
10.5	3 649.935	3 650.671	5 203.331	5 204.097
11.5	3 731.465	3 732.420	5 283.176	5 284.170
12.5	3 819.991	3 821.206	5 369.872	5 371.136
13.5	3 915.492	3 917.009	5 463.396	5 464.975
14.5	4 017.942	4 019.808	5 563.725	5 565.667
15.5	4 127.318	4 129.582	5 670.832	5 673.189
16.5	4 243.591	4 246.306	5 784.689	5 787.516
17.5	4 366.732	4 369.955	5 905.265	5 908.621
18.5	4 496.712	4 500.503	6 032.528	6 036.474
19.5	4 633.497	4 637.919	6 166.443	6 171.046
20.5	4 777.056	4 782.175	6 306.973	6 312.301
21.5	4 927.352	4 933.237	6 454.078	6 460.205
22.5	5 084.348	5 091.073	6 607.718	6 614.719
23.5	5 248.007	5 255.648	6 767.847	6 775.802
24.5	5 418.288	5 426.924	6 934.420	6 943.410
25.5	5 595.149	5 604.864	7 107.385	7 117.499
26.5	5 778.549	5 789.428	7 286.692	7 298.018
27.5	5 968.441	5 980.574	7 472.284	7 484.916
28.5	6 164.780	6 178.261	7 664.105	7 678.138
29.5	6 367.518	6 382.442	7 862.091	7 877.627
30.5	6 576.606	6 593.073	8 066.180	8 083.322

TABLE XV

Calculated Energy Levels for the $[11.6]1.5\,(0)$ and $[11.6]1.5\,(1)$ States of PtD in cm^{-1}

J	$[11.6]1.5\,(0)$		$[11.6]1.5\,(1)$	
	e levels	*f levels*	*e levels*	*f levels*
1.5	11 597.592	11 597.586	13 193.242	13 193.236
2.5	11 615.042	11 615.022	13 210.325	13 210.304
3.5	11 639.469	11 639.423	13 234.240	13 234.190
4.5	11 670.871	11 670.781	13 264.983	13 264.886
5.5	11 709.242	11 709.087	13 302.549	13 302.382
6.5	11 754.575	11 754.329	13 346.932	13 346.667
7.5	11 806.861	11 806.495	13 398.123	13 397.728
8.5	11 866.091	11 865.571	13 456.112	13 455.552
9.5	11 932.253	11 931.541	13 520.887	13 520.122
10.5	12 005.333	12 004.389	13 592.436	13 591.421
11.5	12 085.315	12 084.094	13 670.742	13 669.430
12.5	12 172.184	12 170.638	13 755.790	13 754.128
13.5	12 265.921	12 263.998	13 847.562	13 845.493
14.5	12 366.506	12 364.150	13 946.037	13 943.501
15.5	12 473.916	12 471.071	14 051.196	14 048.126
16.5	12 588.129	12 584.735	14 163.014	14 159.341
17.5	12 709.120	12 705.113	14 281.468	14 277.116
18.5	12 836.862	12 832.177	14 406.533	14 401.420
19.5	12 971.328	12 965.896	14 538.183	14 532.219
20.5	13 112.486	13 106.240	14 676.389	14 669.478
21.5	13 260.307	13 253.174	14 821.124	14 813.159
22.5	13 414.757	13 406.666	14 972.358	14 963.222
23.5	13 575.801	13 566.679	15 130.060	15 119.624
24.5	13 743.405	13 733.177	15 294.201	15 282.320
25.5	13 917.530	13 906.122	15 464.748	15 451.262
26.5	14 098.137	14 085.475	15 641.670	15 626.399

TABLE XVI

Calculated Energy Levels for the [22.9]1.5 (0) and [22.9]1.5 (1) States of PtD in cm^{-1}

J	[22.9]1.5 (0)		[22.9]1.5 (1)	
	e levels	*f levels*	*e levels*	*f levels*
1.5	22 919.797	22 919.797	24 016.504	24 016.504
2.5	22 934.555	22 934.556	24 030.769	24 030.768
3.5	22 955.209	22 955.211	24 050.731	24 050.729
4.5	22 981.752	22 981.755	24 076.384	24 076.379
5.5	23 014.174	23 014.178	24 107.717	24 107.707
6.5	23 052.463	23 052.470	24 144.717	24 144.702
7.5	23 096.606	23 096.617	24 187.370	24 187.347
8.5	23 146.586	23 146.602	24 235.658	24 235.626
9.5	23 202.386	23 202.409	24 289.562	24 289.518
10.5	23 263.985	23 264.017	24 349.060	24 349.001
11.5	23 331.362	23 331.404	24 414.129	24 414.053
12.5	23 404.491	23 404.547	24 484.741	24 484.645
13.5	23 483.348	23 483.420	24 560.869	24 560.748
14.5	23 567.902	23 567.994	24 642.481	24 642.333
15.5	23 658.123	23 658.239	24 729.545	24 729.365
16.5	23 753.978	23 754.123	24 822.024	24 821.808
17.5	23 855.432	23 855.612	24 919.881	24 919.625
18.5	23 962.449	23 962.668	25 023.076	25 022.774
19.5	24 074.988	24 075.255	25 131.566	25 131.214
20.5	24 193.009	24 193.331	25 245.307	25 244.900
21.5	24 316.467	24 316.854	25 364.251	25 363.783
22.5	24 445.318	24 445.778	25 488.350	25 487.814
23.5	24 579.513	24 580.058	25 617.551	25 616.943
24.5	24 719.001	24 719.644	25 751.801	25 751.113
25.5	24 863.732	24 864.486	25 891.043	25 890.270
26.5	25 013.651	25 014.532	26 035.219	26 034.354
27.5	25 168.701	25 169.725	26 184.269	26 183.303
28.5	25 328.823	25 330.009	26 338.128	26 337.056
29.5	25 493.957	25 495.325	26 496.732	26 495.545
30.5	25 664.040	25 665.613	26 660.013	26 658.703

$X\,\Omega = 2.5\ (0)$ ($J = 2.5$, e level) ground state components. It should be noted that we have calculated the *actual* energy separation, not a spin-orbit constant, between the ground state components. The deperturbed, zero-order positions of these states, and hence the true molecular spin-orbit constant, will differ considerably from this value due to the extensive electronic state mixing in PtH.

The least squares fit also yields values of 11 608.17 (± 0.10) cm^{-1} and 11 606.03 (± 0.10) cm^{-1} for the energy separation between the [11.6]1.5 (0) ($J = 2.5$, e level) and $X\,\Omega = 2.5\ (0)$ ($J = 2.5$, e level) states in PtH and PtD, respectively. Interestingly, in PtH, all of the $\Omega = 1.5$ states, with the exception of the [11.6]1.5 (0) and (1) states, have the same f- above e-parity ordering. In PtD a similar situation exists, but in addition to the e- above f-parity ordering in the [11.6]1.5 (0) and (1) states, the relative parity ordering of the [22.9] (1) state is also reversed. A possible explanation for the parity reversal in the [11.6]1.5 (0) and (1) states relative to the X 1.5 (0) and (1) states in both molecules is that a second $\Omega = 0.5$ state ($^2\Sigma^+$ and $^2\Pi_{1/2}$ mixture) is predicted to lie just *above* the [11.6]1.5 state. The close proximity of this state, pushing down rather than up on the $\Omega = 1.5$, may well be responsible for the change in relative parity ordering in these states.

Although our fitting strategy was successful in predicting the positions of many PtH lines, these empirical fits oversimplify the complex interactions between the low-lying PtH molecular states. Since we know that both the upper and lower states are strongly mixed in an Ω, J, and e/f-parity-dependent way, it is not surprising that even when higher-order terms are used, systematic deviations are still present in the residuals. For all the PtH states analyzed so far, we have chosen to model each electronic state in a simplified, approximate formulation and included phenomenological terms to describe other effects in order to have an accurate, predictive model for detecting the

position of the weak PtH features. The PtH states are not simple, well-behaved case (a) states, and consequently we can expect the true molecular constants to differ considerably from our empirically derived values. Despite these inadequacies, however, the B_v and D_v values are in satisfactory agreement with earlier work (see Tables VII and VIII), considering the differences in the fit models used.

B. Perturbation in the 11 941 Å [$\Omega' = 1.5$–$X\Omega'' = 1.5$ (0, 0)] Band of PtD

The low-J lines of the PtD $\Omega' = 1.5$–$X\Omega'' = 1.5$ (0, 0) band are displaced from their predicted positions by a small perturbation in the lower $X\Omega = 1.5$ state. This perturbation is due to interaction of the $X\Omega = 1.5$ (0) state with the $X\Omega = 2.5$ (2) state. Unfortunately, the $v = 2$ vibrational level has not been reported before, so we must extrapolate from the $v = 0$ and 1 levels of the $X\Omega = 2.5$ state. From the observed minus calculated values in Table V, it can be seen that the crossing occurs between the $J = 5.5$ and $J = 6.5$ levels. The spin-uncoupling term, $-B(\mathbf{J}^+\mathbf{S}^- + \mathbf{J}^-\mathbf{S}^+)$, in the rotational Hamiltonian connects the $X\Omega = 1.5$ state with the $X\Omega = 2.5$ state with an off-diagonal matrix element of the form $b(J(J+1)-15/4)^{1/2}$.

A simple fit of the perturbation matrix element and the J-value crossing yields an estimate of 3241.9 cm^{-1} for the separation between the $X\Omega = 1.5$ ($J = 2.5$, $v = 0$), and $X\Omega = 2.5$ ($J = 2.5$, $v = 0$) ground state components, and a value of 0.0259 cm^{-1} for b. This estimate is in very good agreement with the value of 3242.7 cm^{-1} calculated from the laser excitation measurements on PtD. The perturbation analysis and laser excitation data yield values of $T_{1.5}$–$T_{2.5}$ = 3227.2 ($\pm$3) cm^{-1} and 3228.5 ($\pm$0.1) cm^{-1}, respectively, from Eq. (1) for the electronic separation between the X1.5 and X2.5 PtD ground state components, which are both also in excellent agreement with the $T_{1.5}$–$T_{2.5}$ interval of 3224.9 ($\pm$0.1) cm^{-1} derived from the laser excitation measurements on PtH. The difference between the values for the $T_{1.5}$–$T_{2.5}$ electronic separation for PtH and PtD is most likely an artifact due to the incomplete deperturbation of the low-lying electronic states of these molecules rather than an actual electronic isotope shift.

V. DISCUSSION

Using laser excitation and Fourier transform spectroscopy we have identified and linked in energy six of the ten low-lying states of PtH and PtD which originate from the Pt d^9 [^2D] H/D supermultiplet. The locations of all of the known states of PtH are shown in the energy level diagram in Fig. 9. From the $\Omega'' = 1.5$–$X\Omega'' = 1.5$ (0, 0) intercombination bands, it has been possible to experimentally determine the energy separations between the previously unlinked $X\Omega = 1.5$ and $X\Omega = 2.5$ ground state components, and the [11.6]1.5 (0) low-lying state. For PtH, the $X\Omega = 1.5$ and the [11.6]1.5 (0) states lie 3253.7 cm^{-1} and 11 608.2 cm^{-1} (for the $J = 2.5$, e level), respectively, above the $X\Omega = 2.5$ (0) ground state.

The PtH $X\Omega = 1.5$–$X\Omega = 2.5$ spin–orbit interval has been estimated to be $\sim$1200 cm^{-1} by Kaving and Scullman (*2*). Although we derive a spin–orbit splitting which is approximately 2000 cm^{-1} larger than Scullman's estimate, this difference is not surprising since A, the molecular spin–orbit constant, was calculated assuming the $X\Omega = 1.5$ and $X\Omega = 2.5$ components comprise an isolated, noninteracting, inverted $^2\Delta$ state. This estimate neglects other spin–orbit couplings, such as the $\langle {}^2\Delta_{3/2}|H_{SO}|{}^2\Pi_{3/2}\rangle$ interaction, which should be large for molecules containing a third-row transition metal atom. A much larger spin-orbit splitting is consistent with the large atomic

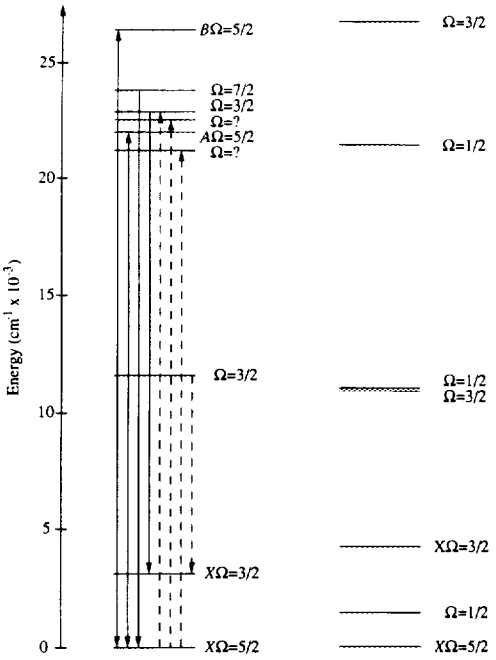

FIG. 9. The electronic states of PtH below 3 eV. The energy levels on the left have been characterized by Scullman and co-workers [see Refs. (*1–3*)] with the exception of the [22.8]?, [21.3]?, and the [11.6]1.5 states reported in the present study. The solid lines indicate those transitions studied previously and the dashed lines are those transitions reported in this work. The theoretical levels on the right were calculated by Balasubramanian and Feng (*11*).

Pt spin–orbit constant [ζ_{5d} = 4221 cm^{-1} (*30*)] and is in better agreement with the recent ab initio calculation by Balasubramanian and Feng (*11*) which places the $X\,\Omega$ = 1.5 component 4200 cm^{-1} above the $X\,\Omega$ = 2.5 ground state.

A second low-lying Ω = 1.5 state has been identified at ~11 600 cm^{-1}. This state appears to correspond to the second lowest Ω = 1.5 state and its T_0 value is in good agreement with the theoretical prediction of 10 850 cm^{-1}. Also, the experimentally determined molecular constants (B_v and $\Delta G_{1/2}$) are consistent with the theoretical trend expected for the two lowest Ω = 1.5 states. The results of both laser excitation and Fourier transform spectroscopy are consistent with the finding that the lower state of the 5089, 5720, 11 935, and 11 876 Å bands is the $X\,\Omega$ = 1.5 state and not the Ω = 0.5 state suggested by Balasubramanian and Feng.

It is very interesting to compare the position and order of the low-lying states of NiH, PdH, and PtH, since Ni, Pd, and Pt all belong to the same subgroup (Group VIII) in the Periodic Table. For NiH, the most extensively studied of the three, the ground state is $^2\Delta_{5/2}$ and the ordering is $^2\Delta < {}^2\Pi \sim {}^2\Sigma^+$; for PdH the ground state is $^2\Sigma^+$ (*31–33*) and the ordering is probably $^2\Sigma^+ < {}^2\Delta < {}^2\Pi$; and finally for PtH, the ground state is again $^2\Delta_{5/2}$ and the ordering is probably $^2\Delta < {}^2\Sigma^+ < {}^2\Pi$. The trend in the electronic symmetry of the ground state and the electronic structure of low-lying states of NiH, PdH, and PtH can be largely explained by two simple atomic factors: (1) the d^9s–d^{10} atomic zero-order separation, and (2) ζ, the atomic spin-orbit coupling constant. Shown in Fig. 10 is a summary of the important atomic parameters for Ni, Pd, and Pt.

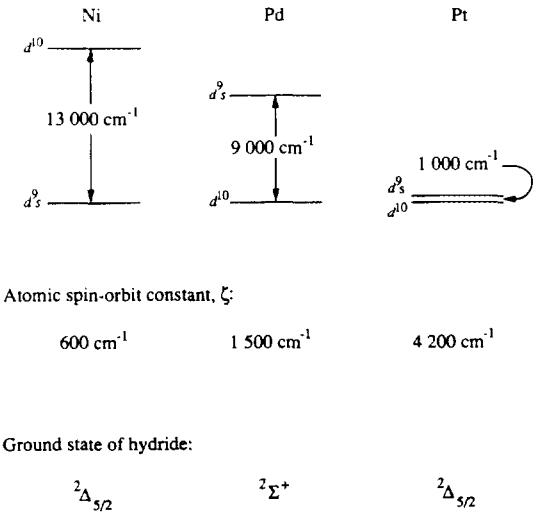

FIG. 10. Atomic parameters for Ni, Pd, and Pt. The zero-order separation between the d^9s and d^{10} atomic configurations is calculated by taking a degeneracy weighted average of the all the individual L–S terms within a single configuration. Atomic spin–orbit constants are taken from Ref. (*30*).

For all three molecules we can assume, to a first approximation, that only the two lowest-lying *atomic* metal-centered electronic configurations d^9s and d^{10} are needed to explain the low-lying *molecular* electronic structure. Although there are other metal atom electronic configurations, most notably d^8s^2, these configurations are sufficiently higher-lying in the free atom that it is more likely that they are responsible for the *excited* state electronic structure in the optical region, rather than the low-lying electronic structure.

The effect of the H ligand on the metal d^9s configuration is difficult to predict because of the mixed ionic–covalent interaction. The bonding is best described as $Pt^{\delta+}$–$H^{\delta-}$ with a $d^9\sigma^2$ configuration (*34*). The large bonding σ orbital has substantial Pt and H character, although, on the basis of the electronegativity difference, it is polarized towards H. The d-hole on Pt gives rise to $d\sigma^{-1}\,{}^2\Sigma^+$, $d\pi^{-1}\,{}^2\Pi$, and $d\delta^{-1}\,{}^2\Delta$ states which are found to be ordered (experimentally and theoretically) $E_\delta < E_\pi < E_\sigma$. On the other hand, the effect of the H ligand on the metal d^{10} configuration can be thought of as simply $M^0(d^{10})\,H^0(1s^1)$. Since the closed d^{10} core is not expected to participate in bonding, there is neither electrostatic stabilization nor destabilization of the resulting $^2\Sigma^+$ molecular state. Therefore, for all three M–H molecules we expect, in the absence of intraconfigurational (spin–orbit effects) and inter-configurational mixing, a priori two zero-order sets of molecular states: a single $d^{10}\,\Sigma^+$ state and three $d^9s\,\Delta$, Π, and Σ^+ states having a deperturbed energy ordering $E_\Delta < E_\Pi < E_{\Sigma^+}$. Via both intraconfigurational (spin–orbit effects between all the states derived from d^9s configuration) and interconfigurational ($d^{10}\,{}^2\Sigma^+ \sim d^9s\,{}^2\Sigma^+$) interactions, the observed, perturbed energy level pattern is produced in each of these molecules.

In the case of Ni, the $3d^{10}$ atomic configuration is located 13 000 cm^{-1} [ΔE given is the degeneracy-weighted average over all L–S terms of the specified configuration (*35*)] above the d^9s ground state configuration. Consequently, in NiH all of the low-lying molecular states are derived predominantly from the d^9s configuration. The $^2\Sigma^+$ state which arises from the $3d^{10}$ atomic configuration interacts only with the $^2\Sigma^+$ state

from the d^9s and causes these two states to mix and repel one another [$\langle 3d^9s|H_{Cl}|3d^{10}\rangle = 11\,650\ cm^{-1}$ (*35*)]. Intraconfigurational mixing also occurs via the molecular spin–orbit [$\zeta_{Ni} = 603\ cm^{-1}$ (*30*)] operator, but since the size of this interaction is small compared to the ligand-field splitting, the positions of the zero-order molecular states are largely preserved and all of the d^9s states are located in a narrow energy range, with an approximate energy level ordering $^2\Delta < {}^2\Pi < {}^2\Sigma^+ < {}^2\Sigma^+_{3d^{10}}$.

For Pd, the $4d^9s$–$4d^{10}$ energy separation is reversed relative to Ni, with the $4d^9s$ state lying almost 9000 cm^{-1} above the $4d^{10}$ state. Although the spin-orbit coupling ($\zeta_{Pd} = 1500\ cm^{-1}$) is larger in Pd than in Ni, PdH can be thought of as NiH "upside down" in the sense that the $^2\Sigma^+$ ground state is mainly d^{10} rather than d^9s. The effect of a larger spin–orbit coupling constant is to increase both intraconfigurational mixing and repulsion among the $4d^9s$ states. Since the zero-order separation between the $4d^{10}$ and $4d^9s$ configurations is a factor of two or three times greater than both the ligand-field splitting among the d^9s sets of states and the spin-orbit coupling constant, the ordering of the low-lying PdH electronic states is again consistent with the zero-order positions of the two atomic configurations and is probably $^2\Sigma^+_{3d^{10}} < {}^2\Delta < {}^2\Pi < {}^2\Sigma^+$, although we would expect the energy spread among the PdH $4d^9s$ states to be larger than in NiH.

In the case of Pt, the $5d^{10}$–$5d^9s$ energy separation is nearly zero. With an even larger atomic spin–orbit constant ($\zeta_{Pt} = 4221\ cm^{-1}$), all of the low-lying states interact strongly via both intra- and interconfigurational terms. In the absence of spin–orbit effects, we might expect the $5d^{10}/5d^9s\ ^2\Sigma^+$ state to be the ground state of PtH because the zero-order positions of the $5d^{10}$–$5d^9s$ configurations are very close in energy and because they interact through a large configuration interaction matrix element. The fact that the ground state of PtH is $^2\Delta_{5/2}$ probably can be explained by two effects: (1) the Δ state is the lowest energy state within the d^9s set of states and (2) intra-configurational spin-orbit interactions will tend to push this state (and $^2\Delta_{3/2}$) down most strongly relative to all the other states in the d^9s configuration. Since the zero-order separation between the d^9s and d^{10} configurations is smaller than the magnitudes of both inter- and intraconfigurational interactions, the observed energy level ordering becomes very difficult to predict.

Studies of PdH, specifically its $^2\Sigma^+$ ground state, should be particularly interesting because this state is derived mainly from the $4d^{10}$ electronic configuration of the Pd atom, unlike all of the low-lying states of NiH and most of the low-lying states of PtH which are metal d^9s in character. A continued study of the PtH low-lying electronic states is also worthwhile because other effects, related to the increased d-orbital size relative to NiH and PdH (*36*), may also be important in this molecule.

VI. CONCLUSIONS

We have observed three new bands of PtH and three new bands of PtD using laser excitation and Fourier transform spectroscopy. Rotational analysis of these bands has allowed us to link in energy three of the five Ω-doubled low-lying electronic states of PtH which are components of the Pt d^9 [^2D] H supermultiplet. The observed states include the $X\,\Omega = 2.5$ and $X\,\Omega = 1.5$ ground state spin–orbit components and another "low-lying" $\Omega = 1.5$ state. Unlike NiH, where all 10 components of the lowest energy d^9 [^2D] supermultiplet are located below about 3000 cm^{-1} (*37*), in PtH, the spacing between all of the low-lying states which have been observed so far spans almost 12 000 cm^{-1}, owing to the large molecular spin–orbit constant which causes very

strong mixing and repulsion between electronic states. At this point we can say very little about either the position of the zero-order, deperturbed PtH electronic states or the atomic configurational parentage of the PtH electronic states. Only when the remaining $\Omega = 0.5$ states are identified and all of the low-lying states are characterized more completely (i.e., Zeeman, Stark, and hyperfine analysis) can a meaningful attempt be made to understand and model the complex interactions in PtH.

ACKNOWLEDGMENTS

M.C.M. and R.W.F. thank Dr. Thomas D. Varberg for helpful discussions. One of the authors (M.C.M.) thanks the AT&T Foundation for an AT&T Bell Laboratories Ph.D. Scholarship. The MIT portion of the research was supported by the National Science Foundation under Grants CHE86-14437 and CHE91-20329.

R.E. and P.B. thank the National Solar Observatory, operated by the Association of Universities for Research in Astronomy, Inc., under contract with the National Science Foundation, for the use of the McMath Fourier transform spectrometer. They also thank J. Wagner, G. Ladd, and J. W. Brault for help in obtaining the spectra. Acknowledgment is also made to the Petroleum Research Fund administered by the American Chemical Society, for partial support of this work. P.B. also thanks the Natural Science and Engineering Research Council of Canada for support.

RECEIVED: September 3, 1992

REFERENCES

1. R. SCULLMAN, *Ark. Fys.* **28,** 255–265 (1964).
2. B. KAVING AND R. SCULLMAN, *Can. J. Phys.* **49,** 2264–2275 (1971).
3. R. SCULLMAN AND P. CEDERBALK, *J. Phys. B* **10,** 3659–3664 (1977).
4. H. NEUHAUS AND R. SCULLMAN, *Z. Naturforsch. A* **19,** 659–660 (1964).
5. B. KAVING AND R. SCULLMAN, *Phys. Scr.* **9,** 33–39 (1974).
6. G. GUSTAFSSON AND R. SCULLMAN, *Mol. Phys.* **67,** 981–988 (1989).
7. S. W. WANG AND K. S. PITZER, *J. Chem. Phys.* **79,** 3851–3858 (1983).
8. A. GAVEZZOTTI, G. F. TANTARDINI, AND M. SIMONETTA, *Chem. Phys. Lett.* **129,** 577–581 (1986).
9. S. TOBISCH AND G. RASCH, *Chem. Phys. Lett.* **166,** 311–316 (1990).
10. C. M. ROHLFING, P. J. HAY, AND R. L. MARTIN, *J. Chem. Phys.* **85,** 1447–1455 (1986).
11. K. BALASUBRAMANIAN AND P. Y. FENG, *J. Chem. Phys.* **92,** 541–550 (1990).
12. M. TRKULA, D. O. HARRIS, AND R. C. HILBORN, *Chem. Phys. Lett.* **93,** 345–349 (1982).
13. T. D. VARBERG, E. J. HILL, AND R. W. FIELD, *J. Mol. Spectrosc.* **138,** 630–637 (1989).
14. J. CARIOU AND P. LUC, "Atlas du Spectre d'Absorption de la Molecule de Tellure," CNRS II, Orsay, France.
15. R. ENGLEMAN, JR., *J. Opt. Soc. Am. B* **2,** 1934–1941 (1985).
16. R. ENGLEMAN, JR., R. D. COWAN, AND J. M. PEEK, *J. Opt. Soc. Am. B* **5,** 2294–2297 (1988).
17. J. W. BRAULT, *J. Opt. Soc. Am.* **66,** 1081 (1976); J. W. BRAULT, *Osserv. e Mem. dell Osserv., Astron. di Arcetri.* **106,** 33 (1979).
18. B. A. PALMER AND R. ENGLEMAN, JR., "Atlas of the Thorium Spectrum," Los Alamos National Laboratory report, LA-9615, 1983.
19. J. A. GRAY, Ph.D. Thesis, MIT, 1988.
20. R. R. SQUIRES, *J. Am. Chem. Soc.* **107,** 4385–4390 (1985).
21. C. LINTON, M. DULICK, R. W. FIELD, P. CARETTE, P. C. LEYLAND, AND R. F. BARROW, *J. Mol. Spectrosc.* **102,** 441–497 (1983).
22. A. LAGERQVIST AND R. WESTÖÖ, *Ark. Mat. Astron. Fys.* **32A,** No. 10 (1945).
23. G. HERZBERG, "Molecular Spectra and Molecular Structure. I. Spectra of Diatomic Molecules," 2nd ed., Van Nostrand–Reinhold, New York, 1950.
24. C. H. TOWNES AND A. L. SCHAWLOW, "Microwave Spectroscopy," McGraw–Hill, New York, 1955.
25. A. G. ADAM, Y. AZUMA, J. A. BARRY, G. HUANG, M. P. J. LYNE, A. J. MERER, AND J. O. SCHRÖDER, *J. Chem. Phys.* **86,** 5231–5238 (1987).
26. S. FRAGA, J. KARWOWSKI, AND K. M. S. SAXENA, "Handbook of Atomic Data," Elsevier, Amsterdam, 1975.

27. I. KOPP AND J. T. HOUGEN, *Can. J. Phys.* **45,** 2581–2596 (1967).
28. R. S. MULLIKEN, *Rev. Mod. Phys.* **3,** 89 (1931).
29. J. M. BROWN, A. S-C. CHEUNG, AND A. J. MERER, *J. Mol. Spectrosc.* **124,** 464 (1987).
30. H. LEFEBVRE-BRION AND R. W. FIELD, "Perturbations in the Spectra of Diatomic Molecules," Academic Press, New York, 1986.
31. K. BALASUBRAMANIAN, P. Y. FENG, AND M. Z. LIAO, *J. Chem. Phys.* **87,** 3981–3985 (1987).
32. C. MALMBERG, R. SCULLMAN, AND P. NYLÉN, *Ark. Fys.* **39,** 495–510 (1968).
33. L. B. KNIGHT, JR., AND W. WELTNER, JR., *J. Mol. Spectrosc.* **40,** 317–327 (1971).
34. S. F. RICE, H. MARTIN, AND R. W. FIELD, *J. Chem. Phys.* **82,** 5023–5034 (1985).
35. J. A. GRAY, M. LI, TH. NELIS, AND R. W. FIELD, *J. Chem. Phys.* **95,** 7164–7178 (1991).
36. E. M. SPAIN AND M. D. MORSE, *J. Chem. Phys.* **97,** 4605–4615 (1992).
37. J. A. GRAY, M. LI, AND R. W. FIELD, *J. Chem. Phys.* **92,** 4651–4659 (1990).